Systematic Comparison of Hydrogen-Tank Layouts in Blended Wing Body Aircraft

Maximilian Voss* and Benjamin M.H.J. Fröhler† and Thomas Zill‡

Institute of System Architectures in Aeronautics, German Aerospace Center, Hamburg, Germany

Maurice F.M. Hoogreef§

Faculty of Aerospace Engineering, Delft University of Technology, Delft, The Netherlands

Hydrogen-fueled aircraft can substantially reduce climate impact compared to their kerosene-powered counterparts, yet hydrogen's low volumetric density, four times lower than that of liquid kerosene, poses significant integration challenges. Blended-wing-body (BWB) configurations have been proposed as a more suitable platform for hydrogen storage than conventional tube-and-wing (TAW) designs. However, no systematic comparison of different hydrogen-tank configurations against a consistent kerosene baseline exists. Therefore, this study evaluates four hydrogen-tank layouts identified in prior research against a kerosene-powered BWB baseline, and against equivalent TAW configurations, under common top-level aircraft requirements (TLAR): 2500 nmi range and 239 passengers, with 2050 entry into service technology assumptions. The objective is to assess the installation penalty of hydrogen tanks on BWB design and the suitability of this platform for hydrogen tank integration. Using conceptual design methods, each BWB design was specifically tailored to its tank configuration and then ranked by block-energy penalty. The tank layout with an integration adjacent to, and aft of, the cabin incurred the lowest penalty (12.5 %) among BWB options, but still exceeded the 10.5 % penalty of the TAW counterpart. Sensitivity analyses varying integration assumptions confirmed the consistency of this finding. These findings do not eliminate hydrogen-fueled BWB aircraft as a viable alternative to hydrogen-fueled TAW designs, as literature shows that BWB configurations still offer an inherent efficiency advantage. However, their higher integration penalty must be considered in the overall trade-off.

Nomenclature

Latin Symbols

AR	=	Wing aspect ratio [-]
c_1, c_2, c_3, c_4	=	Clearance length [m]
$c_{L_{\alpha,w}}$	=	Wing lift-curve gradient [-]
d	=	Diameter [m]
d_n	=	Nacelle diameter [m]
k_n	=	Nacelle integration factor [-]
l	=	Length [m]
m	=	Mass [kg]
n_{eng}	=	Number of engines [-]
S	=	Wing area [m^2]
v	=	Volume [m^3]
x	=	Longitudinal position [m]
y	=	Lateral position [m]

Greek Symbols

η_g	=	Gravimetric efficiency [-]
η_v	=	Volumetric efficiency [-]
$\phi_{sec,ref}$	=	Reference secondary mass fraction [-]

Subscripts

cab	=	Cabin
fus	=	Fuselage
H2	=	Hydrogen
transition	=	Transition wing
unpress	=	Unpressurized aft segment

Abbreviations

AMC	=	Aircraft Mission Calculator
BWB	=	Blended Wing Body
CAS	=	Calibrated Airspeed
CFD	=	Computer Fluid Dynamics
CFRP	=	Carbon Fiber-Reinforced Polymer
COG	=	Center of Gravity

*Research Engineer, Air Vehicle Concepts and Impact Assessment

†Research Engineer, Air Vehicle Concepts and Impact Assessment

‡Head of Air Vehicle Concepts and Impact Assessment, Senior member AIAA

§Assistant Professor, Faculty of Aerospace Engineering, Senior member AIAA

DC	=	Drag Counts	MLM	=	Maximum Landing Mass
DLR	=	German Aerospace Center	MTOM	=	Maximum Take-Off Mass
EIS	=	Entry into Service	MZFM	=	Maximum Zero-Fuel Mass
FEA	=	Finite Element Analysis	OEM	=	Operating Empty Mass
FLOPS	=	Flight Optimization System	RCE	=	Remote Component Environment
HTP	=	Horizontal Tail Plane	SL	=	Sea-Level
ICAO	=	International Civil Aviation Organization	SMR	=	Short/Medium Range
LH_2	=	Liquid Hydrogen	TAW	=	Tube-and-Wing
ISA	=	International Standard Atmosphere	TLAR	=	Top-level Aircraft Requirement
LoD	=	Lift to Drag	UHBPR	=	Ultra-high Bypass Ratio
MAC	=	Mean Aerodynamic Chord	VELA	=	Very Efficient Large Aircraft
MER	=	Mass Estimation Relationship			
MLI	=	Multilayer insulation			

I. Introduction

The aviation industry is a significant contributor to global warming, accounting for 3.5 % of total anthropogenic effective radiative forcing in 2018 [1]. One promising technological solution for significantly reducing climate impact is the development of hydrogen-fueled aircraft. Compared to kerosene, hydrogen does not result in direct CO_2 emissions, and its production can be climate-neutral. However, in the early stages of adopting hydrogen-fueled aircraft, climate-neutral hydrogen will be scarce and expensive [2]. While early studies have found that hydrogen-fueled tube-and-wing (TAW) aircraft are more efficient than kerosene-fueled TAW aircraft [3], later studies suggest that hydrogen aircraft are less efficient [4] and sensitive to tank integration/location [5]. Thus, even with carbon-neutral hydrogen fuel, efforts must continue to improve aircraft efficiency and reduce energy consumption.

The conventional TAW configuration has been optimized for over 70 years [6], so attention shifts to radically different unconventional configurations that aim to significantly lower fuel consumption and climate impact. One notable unconventional design is the blended wing body (BWB) configuration, envisioned at McDonnell Douglas by Liebeck et al. [7] in 1988. By integrating the lift-generating wing and passenger-accommodating fuselage, the BWB increases its aerodynamic efficiency relative to the TAW configuration. Numerous detailed design studies on the BWB have been performed, such as those at McDonnell Douglas/Boeing [7] and the European Very Efficient Large Aircraft (VELA) project [8]. These studies have found significant improvements in overall aircraft efficiency relative to TAW aircraft configurations.

Several authors [9, 10] note that the BWB shape lends itself particularly well to the integration of liquid hydrogen (LH_2) tanks, and a number of studies have been conducted to investigate the performance impact of LH_2 integration on BWB aircraft. Relative to a kerosene-fueled BWB baseline aircraft, Karpuk et al. [11] and Nguyen Van et al. [12] found that the LH_2 BWB is less efficient. Adler and Martins [13] found that the LH_2 BWB is less efficient than its kerosene counterpart for all but very high gravimetric efficiencies, and Chan et al. [14] report that the LH_2 BWB only outperforms the kerosene configuration for ranges exceeding 6000 nmi, which is in agreement with Jagtap et al. [10] for a similarly sized aircraft. However, compared to TAW aircraft, studies on LH_2 integration in BWB designs are still scarce, and several gaps remain in the current literature. While the BWB offers considerable flexibility for integrating LH_2 tanks, as shown by the variety of LH_2 tank integrations investigated [10–17], direct comparisons of different tank layouts under identical top-level aircraft requirements (TLAR) are lacking [13] except for a recent study by Di Summa [17].

In addition, in most studies, tank mass is estimated using fixed gravimetric efficiency values [10, 12, 13, 15], without accounting for the impact of the specific tank geometries. Different tank layouts may, however, significantly change the relative tank mass between differing tank layouts and relative to the TAW configuration. A physics-based modeling approach, as utilized by Karpuk et al. [11] and Di Summa [17], is necessary to accurately capture the effects of different tank layouts on the gravimetric efficiency and thus aircraft performance.

It was also observed that most studies either omit the assumed technology level or consider a 2035 horizon at most, which appears unrealistic for the simultaneous introduction of both the BWB configuration and LH_2 as an energy carrier. This is reflected in Airbus' decision to delay the development of its TAW LH_2 aircraft beyond 2035 [18], underscoring the need for research based on more plausible entry into service (EIS) timelines.

Furthermore, performance assessments often compare LH_2 BWB concepts to kerosene-fueled BWB or TAW aircraft with inconsistent technology assumptions [10–12, 15], limiting the validity of such comparisons. Although a wide range of capacities and ranges has been studied, few designs align with the short/medium range (SMR) segment currently

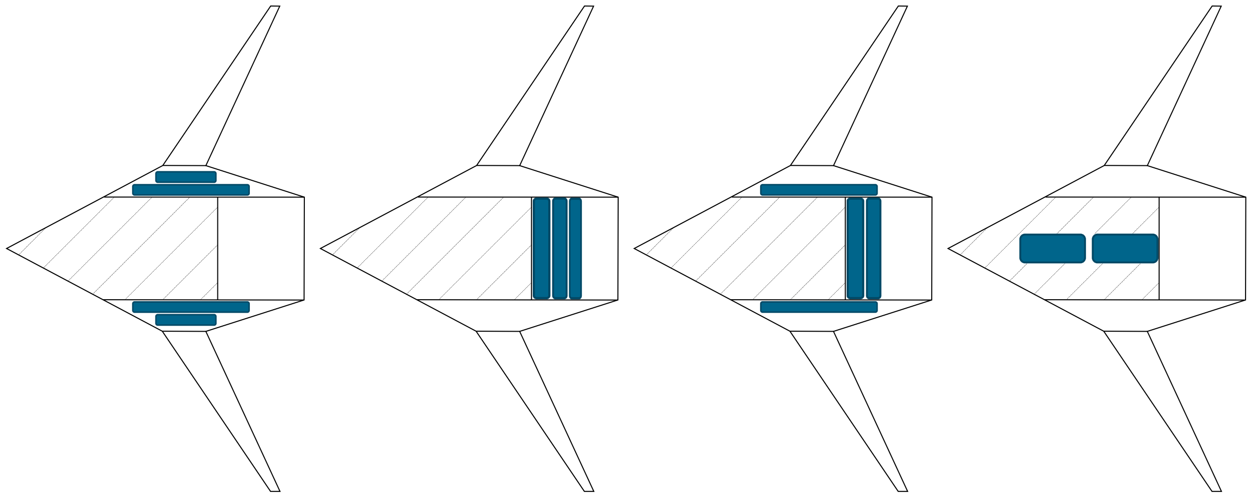

(a) Lateral tank layout. **(b) Aft tank layout.** **(c) Combined tank layout.** **(d) Center tank layout.**

Fig. 1 Sketches of BWB LH_2 tank layout with tanks visualized in blue.

prioritized for future developments by Airbus and Boeing. With Airbus and JetZero proposing BWB concepts for 200 to 250 passengers [19, 20], further work is needed to assess LH_2 BWB aircraft under comparable TLAR.

Building on previous research and addressing the identified research gaps, the present study seeks to contribute to the evaluation of different hydrogen-fueled BWB configurations. For this purpose, an LH_2 tank-sizing methodology is integrated into an existing conceptual aircraft design environment to enable a direct comparison of kerosene- and LH_2 fueled TAW and BWB aircraft. LH_2 configurations are generated for both the BWB and TAW designs under consistent TLAR and technology assumptions, aligned with a 2050 EIS. To assess the relative LH_2 integration penalties of these configurations, corresponding kerosene-fueled baseline aircraft are developed. Ultimately, the goal of this study is to answer the following research question:

How do different tank layouts impact the energy consumption of a hydrogen-fueled BWB aircraft compared to a kerosene-fueled BWB under consistent top-level aircraft requirements and technology level assumptions?

Figure 1 visualizes the four different tank layouts evaluated in this study. In addition to the "lateral," "aft," and "combined" tank layout assessed in previous work [10–17], a fourth "center" tank layout is investigated. A layout similar to this was proposed by Adler and Martins [21] but has not yet been evaluated. The lateral and aft tank layouts represent extremes of the combined tank layout and are assessed separately to account for scenarios in which evacuation, manufacturing, or other integration constraints might invalidate the combined tank layout.

This paper is structured as follows. Section II describes the methodological framework. Section III introduces the kerosene reference aircraft as well as the baseline TAW and BWB configurations used as performance benchmark. The integration of liquid hydrogen and its aircraft design approach are presented in Section IV. Section V compares the performance of the LH_2 TAW and BWB configurations, focusing on hydrogen integration penalties and key performance metrics. In Section VI, the findings are placed in the context of existing literature to assess their plausibility and to support validation. Finally, Section VII summarizes the main conclusions and outlines recommendations for future research.

II. Methodology

A multidisciplinary, integrated aircraft design workflow is developed to evaluate both the TAW and the BWB with kerosene and LH_2 as an energy carrier. To ensure comparability, the workflow maintains a high degree of consistency across all configurations. It integrates a set of design and analysis tools developed internally within the German Aerospace Center's (DLR) aircraft design environment.

This environment is hosted in the Remote Component Environment (RCE) [22], which enables the seamless coupling of diverse tools into a continuous workflow. Communication between workflow components is managed through DLR's

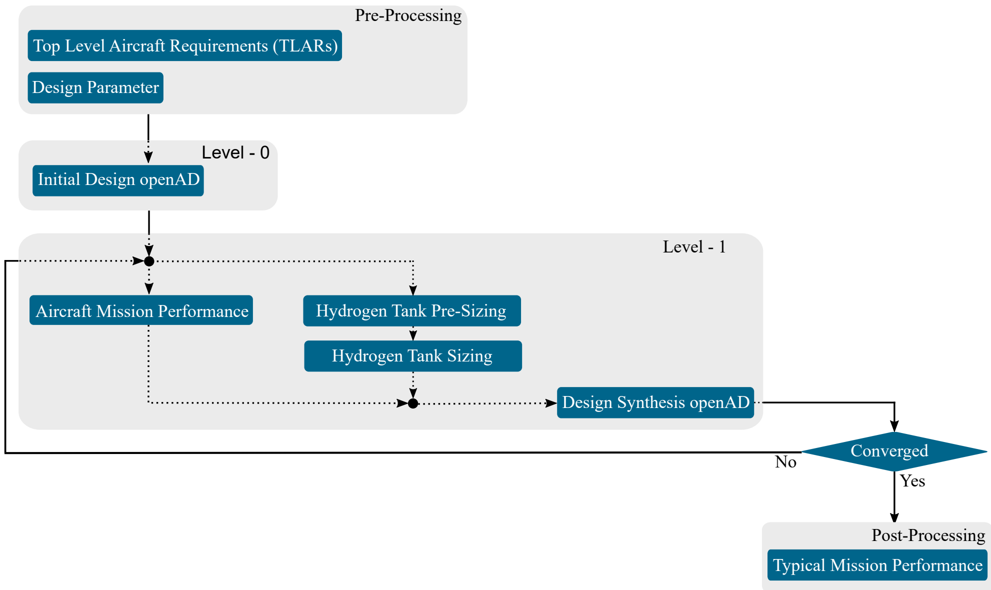

Fig. 2 Flowchart of the aircraft design process.

Common Parametric Aircraft Configuration Schema (CPACS) [23], which provides a standardized format for exchanging data such as aerodynamic polars, engine performance maps, airfoil profiles, masses, and geometric definitions.

The workflow consists of four main stages visualized in Fig. 2: pre-processing of input parameters, an initial low-fidelity design phase, an iterative design loop using higher-fidelity methods, and post-processing.

The process begins with a set of TLAR's provided by the user (see Chapter III) and additional design parameters depending on the specific configuration. The DLR internal conceptual aircraft design tool openAD [24] then generates an initial aircraft concept based on low-fidelity methods.

This initial design is then evaluated with higher-fidelity tools for mission analysis and LH_2 tank sizing. The LH_2 tank sizing process is divided into two steps. For the BWB configuration, an additional pre-sizing step is required to prepare the geometry for use with the standardized LH_2 tank sizing tool. This tool then computes the mass and geometrical properties of the tank.

Design synthesis is subsequently performed in an iterative loop until convergence is reached. Convergence is defined by an absolute error below 10 kg or a relative error below 0.05 % in maximum take-off mass (MTOM), operating empty mass (OEM), and block fuel. For LH_2 configurations, cabin length and bulkhead height are included as additional convergence variables. The final output is a fully defined aircraft concept, including geometry, aerodynamic characteristics, mass properties, propulsion data, and performance metrics.

In the following, the applied methods are described more in detail, distinguishing between the TAW and BWB configurations. Including the mission analysis tool, and the LH_2 tank sizing and integration process.

A. Tube-and-Wing Conceptual Aircraft Design Module

At the core of the workflow is the conceptual aircraft design tool openAD. It integrates low-fidelity handbook methods [25–27], as well as methods developed internally at DLR. Rather than performing an optimization, openAD generates a feasible and consistent aircraft design based on a set of user-defined TLAR. A detailed description of the methods, along with validation across a wide range of aircraft types, is provided by Wöhler et al. [24].

OpenAD is extended to integrate LH_2 tanks aft of the cabin. Accommodating these tanks requires additional fuselage volume, achieved by increasing the fuselage length, diameter, or both. The structural mass estimation in openAD has therefore been adapted to account for the modified aft fuselage. While the LH_2 tank itself is designed and evaluated using a separate tool, openAD estimates the fuselage mass based on an empirical method from the Luftfahrtechnisches Handbuch [28]. This method originally includes secondary structure along the entire fuselage. When an LH_2 tank is installed in the aft section, this secondary structure becomes unnecessary. To reflect this, Balack et al. [29] introduced a correction factor applied to the fuselage structural mass:

$$f = 1 - \phi_{\text{sec,ref}} + \phi_{\text{sec,ref}} \cdot \frac{l_{\text{fus,ref}}}{l_{\text{cab,ref}}} \cdot \frac{l_{\text{cab}}}{l_{\text{fus}}}, \quad \text{where} \quad \phi_{\text{sec,ref}} = \frac{m_{\text{sec,ref}}}{m_{\text{fus,ref}}}. \tag{1}$$

Here, f is the correction factor, and $\phi_{\text{sec,ref}}$ is the secondary structure mass fraction of a reference aircraft, calculated from the mass of the secondary structure $m_{\text{sec,ref}}$ and the total fuselage structural mass $m_{\text{fus,ref}}$. The parameter $l_{\text{fus,ref}}$ and $l_{\text{cab,ref}}$ denote the fuselage and cabin lengths of the reference aircraft, respectively, while l_{fus} and l_{cab} refer to the lengths of the actual aircraft. This factor adjusts the fuselage mass to reflect the reduced length requiring secondary structure. The method shows good agreement with higher-fidelity results and has been integrated into openAD. A similar correction by Balack et al. [29] has also been implemented for estimating the fuselage structure's center of gravity (COG).

B. Blended Wing Body Conceptual Aircraft Design Module

The BWB module in openAD builds on existing methods from the TAW module wherever applicable. However, the distinct configuration necessitated substantial modifications to geometry and sizing, aerodynamics, mass estimation, propulsion modeling, and static stability analysis.

Geometry and Sizing

The BWB is divided into three wing regions, the inner wing, the transition wing, and the outer wing, and is then further divided into six segments, as visualized in Fig. 3. The inner wing region includes a pressurized segment for passengers and crew, and an unpressurized segment aft of the rear bulkhead. The transition wing connects the inner to the outer wing, which is defined to resemble the wing of the TAW configuration [24].

The BWB's planform (Fig. 4) is sized according to passenger capacity and geometric constraints. The required cabin planform area is determined from the passenger number and a passenger density*. Its dimensions are defined by either a prescribed width w_{cab} or a length-to-width ratio, together with the leading-edge sweep angle. A cockpit segment, sized from a reference aircraft, is added in front of the cabin. Based on these dimensions, the inner wing geometry is derived, with its leading edge aligned to the cabin wall. To ensure passenger accommodation, a minimum bulkhead height h_{bulk} must be maintained at both the center and cabin stations (Fig. 5). This requirement determines the

*Passengers per unit cabin area

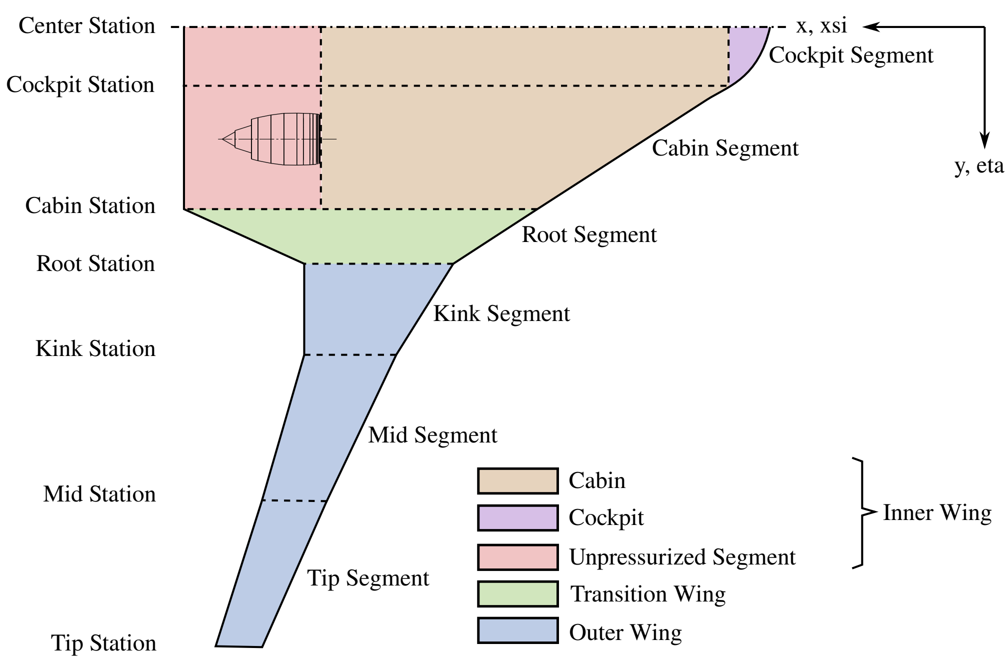

Fig. 3 BWB geometry definition.

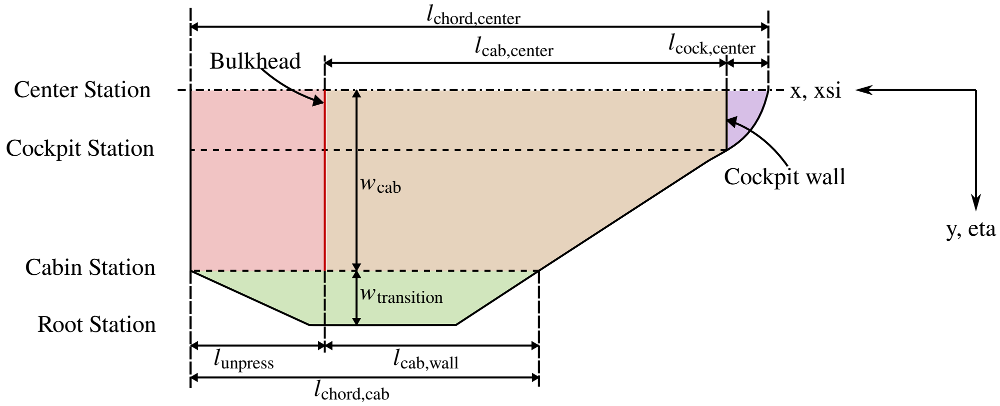

Fig. 4 BWB inner wing and cabin planform definition.

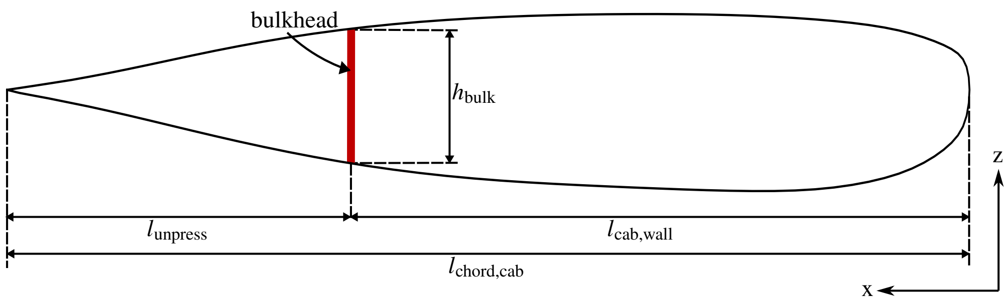

Fig. 5 BWB side-view at the cabin station showing the definition of the bulkhead height.

unpressurized aft length $l_{unpress}$ and the necessary chord lengths at the center and cabin stations ($l_{chord,center}$, $l_{chord,cab}$). The inner wing trailing edge and rear bulkhead are unswept.

The total wing area is determined using the same methodology as for the TAW configuration [24], typically constrained by landing field length requirements. From the total wing area S, the outer wing reference area S_{outer} is calculated as

$$S_{outer} = S - S_{inner} - S_{transition}, \tag{2}$$

where S_{inner} and $S_{transition}$ are the reference areas of the inner and transition wing segments, respectively. The transition wing reference area is determined implicitly by the geometries of the inner and outer wing. The width of the transition wing $w_{transition}$ is defined relative to the wingspan and provided as a user-input.

For LH_2 configurations (Fig. 1), tanks are integrated into the inner and/or transition wings, significantly increasing their area. When total wing area is constrained by landing requirements, this may result in unrealistically small spans or excessive outer wing aspect ratios. To ensure feasible designs, limits on maximum outer wing aspect ratio and/or wingspan can be imposed. If these limits are exceeded, the outer wing area or span is adjusted accordingly. The remaining outer wing geometry is defined following the TAW methodology of Wöhler et al. [24].

Aerodynamics

Aerodynamic analysis is performed using low-fidelity methods in openAD. These are calibrated against high-fidelity results from a reference aircraft introduced in Chapter III to improve absolute accuracy and are primarily applied to capture sensitivities to design changes. The zero-lift drag coefficient C_{D_0} is estimated using the component build-up method from Raymer [25], which estimates the drag based on a component form factor and the flat plate friction drag. Wave drag C_{D_w} is approximated using a combination of methods from Torenbeek [26, 30]. These methods account for drag due to equivalent 25 % sweep, mean wing thickness, and lift coefficient at the current flight point. The induced drag coefficient C_{D_i} is calculated from the Oswald efficiency factor e following Raymer [25].

Mass Estimation

The structural design of BWBs is distinctly different and require specific methods for mass estimation. For mass estimation, the wing is partitioned as shown in Fig. 3.

The mass of the pressurized inner wing segment is calculated using the method developed by Bradley and Kimmel [31], which correlates structural mass with cabin area and MTOM. This approach is based on a regression fit to finite element analysis (FEA) data calibrated against detailed Boeing studies. The mass of the unpressurized aft segment of the inner wing is estimated using the same author's mass estimation relationship (MER), treating the segment as a horizontal tail and applying a correction for the number of engines attached. For the outer wing, the method by Howe [32] is adopted, idealizing the planform as described therein. Since this study does not include a detailed BWB structural layout, the fraction of the root chord occupied by the structural box is approximated as 0.5, following Howe [33]. Initially, following Howe [32], the transition wing was grouped with the outer wing for mass estimation. However, integrating LH_2 fuel tanks in the transition wing leads to significant changes in its planform. It was found that the method of Howe [32] predicts only modest wing mass changes, likely underestimating the effects of transition wing size variations. Instead, the method of Bradley and Kimmel [31] for the unpressurized aft segment is applied to the transition wing, as proposed by Di Summa [17]. In addition, for LH_2 tank integration, the mass penalty for engine integration proposed by Howe [32] is applied per LH_2 tank to the mass of the unpressurized aft segment or the transition wing, respectively.

Propulsion

The engine-cycle calculations for the BWB are identical to those used for the TAW configuration, based on a simplified analytical method detailed by Wöhler et al. [24]. The engines are located at the aft of the inner wing. As lateral stability is not considered in this study, the engine's lateral position is fixed halfway toward the transition wing, and its longitudinal position is defined by the bulkhead location. For the LH_2 BWB configurations, the lateral engine position remains equal to that of the kerosene configuration. However, the longitudinal position varies with the tank layout. To prevent disk strike, the engine is placed such that the fan aligns with the aftmost tank position.

Static Stability

The static longitudinal stability is evaluated using low-fidelity methods. To evaluate the static longitudinal stability, the neutral point and the COG need to be obtained. The COG at different flight points is obtained from the component COG. Following de Castro [34], the neutral point of the BWB configuration is approximately equal to its aerodynamic center. For subsonic flight, the aerodynamic center of a wing is at approximately the quarter-chord location [25]. According to Torenbeek [26], the longitudinal shift in aerodynamic center due to nacelle installation $\Delta x_{\mathrm{ac,n}}$ can be estimated as

$$\Delta x_{\mathrm{ac,n}} = n_{\mathrm{eng}} \cdot k_{\mathrm{n}} \cdot \frac{d_{\mathrm{n}}^2 \cdot l_{\mathrm{n}}}{S \cdot C_{L_{\alpha,w}}}. \tag{3}$$

Here, n_{eng} is the number of installed engines, d_{n} is the nacelle diameter, l_{n} is the distance from the wing quarter-chord to the nacelle, S is the wing reference area, and $C_{L_{\alpha,w}}$ is the wing lift-curve slope. k_{n} is the nacelle integration factor, where the value of -2.5 for aft-fuselage mounted engines is also applied for the aft-mounted engines on the BWB.

C. Aircraft Performance Analysis

The performance of the aircraft configuration is evaluated using the Aircraft Mission Calculator (AMC) [24]. Energy consumption during taxiing, take-off, approach, and landing is estimated based on fuel fractions, while high-speed performance is assessed by solving two-dimensional equations of motion. An optimization is performed to determine the optimal initial cruise altitude and the optimal stepwise climb profile. For this purpose, the tool uses engine performance data and aerodynamic polar. The location of the step climb is selected to minimize energy consumption. The tool outputs fuel requirements for each flight phase and provides key cruise performance indicators such as the cruise lift coefficient and lift to drag (LoD)-ratio. In post-processing, the tool can be used to obtain the payload-range characteristics of the aircraft.

D. LH2 Tank Integration

In the following, the common LH_2 tank sizing routine used for both the TAW and BWB configurations is introduced. Integrating the LH_2 tanks into the BWB configurations requires a pre-sizing step to determine the tank layout. These pre-sizing routines are then discussed for each of the four BWB LH_2 tank layouts.

LH2 Tank Sizing

The LH_2 tanks are sized using the process described by Burschyk et al. [35], which is enhanced by a structural analysis developed by Freund et al. [36]. The tanks feature a cylindrical main section with torispherical end caps and optionally include a conical segment. As shown in Fig. 6, the total tank length l_{tank} consists of the cylindrical length l_{cyl} and the conical length l_{con}. The cylindrical diameter is denoted by d_{cyl}, and d_{con} defines the diameter at the end of the conical section. The multilayer insulation (MLI)-insulated carbon fiber-reinforced polymer (CFRP) tanks consist of an inner shell exposed to the LH_2 , the MLI layer, a vacuum layer, and an outer shell.

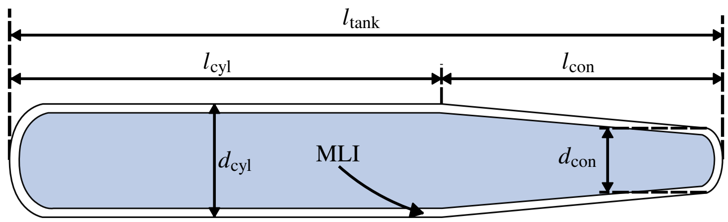

Fig. 6 LH2 tank parameterization.

The total storage mass includes the masses of the inner and outer CFRP shells, the MLI, structural attachments between the shells, fuselage attachment points, and a crash structure. The mass of the CFRP shells is estimated using a surrogate model based on the cylindrical length, length-to-radius ratio, and maximum differential pressure. The differential pressure on the inner shell corresponds to the LH_2 pressure, while the outer shell is sized for the external atmospheric pressure. The surrogate, calculated using the tool tankoh2 [37], sizes the shells for inter-fiber failure. To account for thermal fatigue effects, a safety factor of two is applied to the shell mass predictions. The MLI mass is computed from the tank surface area and an assumed area density. Attachment masses are estimated based on the total mass of the inner shell and the total hydrogen mass, and the crash structure mass is calculated as a function of the total tank mass.

Tank sizing is based on the usable fuel mass and includes additional volume for ullage, unusable fuel, internal structures, pressurization, and contraction effects. Ullage is defined as a percentage of the real tank volume, while contraction and internal structure volume are specified as fractions of the ideal tank volume. The unusable fuel is defined as a percentage of the total fuel mass. Pressurization fuel is computed through thermodynamic analysis, accounting for the additional gaseous hydrogen needed to maintain constant internal pressure as fuel is withdrawn.

An important requirement for LH_2 tanks is the dormancy requirement, which specifies how long the tank can withstand pressure increases from inevitable hydrogen boil-off without venting. Dormancy is not considered in this study, as it has been shown to have only a minor impact on the mass of MLI-insulated tanks. Sielemann et al. [38] demonstrated that increasing the dormancy requirement from 8 to 16 hours has a negligible effect on the mass of such tanks with capacities above 100 kg of hydrogen.

To ensure feasible tank layouts, constraints are applied on the minimum tank diameter and the maximum tank aspect (length-to-diameter) ratio. A minimum diameter of 0.8 m for the cylindrical segment of the tank and a maximum aspect ratio of 10 are imposed. These limits help avoid infeasible designs.

For the performance assessment of different LH_2 tank layouts, the sensitivity of tank mass to changes in tank geometry is essential. To evaluate this sensitivity, a fixed volume is prescribed while tank aspect ratio is changed. The gravimetric efficiency η_g serves as a metric for mass efficiency and is defined as

$$\eta_g = \frac{m_{H_2}}{m_{H_2} + m_{\text{tank}}}, \tag{4}$$

where m_{H_2} is the usable LH_2 mass and m_{tank} is the total tank mass, including attachments, crash structures, and additional unusable fuel masses.

Figure 7 shows the predicted gravimetric efficiency for a fixed usable fuel mass of 500 kg over a range of length-to-diameter ratios, illustrating the expected decline in gravimetric efficiency for more slender configurations. From Fig. 7, it can be seen that the highest gravimetric efficiency is achieved for a tank with a length-to-diameter ratio of approximately one. For these configurations, the tank is closest to a sphere, which, for a given volume, has the lowest surface-area-to-volume ratio. As the length is increased and the diameter decreased, the surface-area-to-volume ratio increases, leading to an increase in tank mass.

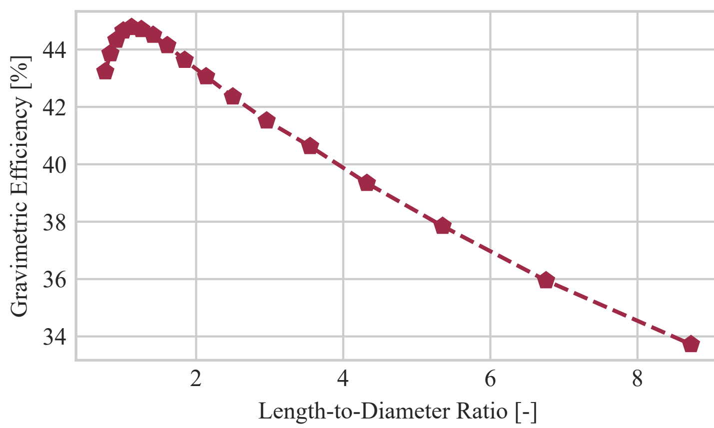

Fig. 7 Gravimetric efficiency of LH2 tanks for varying length-to-diameter ratios for 500 kg usable hydrogen mass.

LH2 Tank Pre-Sizing for BWB Configurations

Four different tank layouts for the BWB configuration, i.e. "lateral," "aft," and "combined" tank layouts as well as the "center" tank, are identified from literature [10–17]. In order to fit the different tank layouts into the BWB, a pre-sizing is required.

For the lateral tank layout (see Fig. 1a), the LH_2 tanks are positioned within the transition wing. Integrating the tanks into this region requires a modification of the wing planform geometry. As illustrated in Fig. 4, for a constant cabin area, increasing the cabin length along the centerline reduces the width of the inner wing while increasing both the width and length of the transition wing, assuming a fixed root station. Based on this relationship, the planform was adapted by varying the cabin length while keeping the lateral position of the root station constant. The lateral tank sizing procedure is based on a scalar root-finding approach that determines the cabin length required to accommodate the specified fuel volume within the transition wing. The objective is to identify the cabin length for which the cumulative volume of all lateral tanks matches the required fuel volume. For each iteration of the cabin length, the geometry of the transition wing planform is recalculated to reflect the updated configuration. The tanks are arranged symmetrically on either side of the passenger cabin and separated from surrounding structures by prescribed clearances. As illustrated in Fig. 8, c_1 defines the minimum clearance to the upper airfoil surface, c_2 the spacing between adjacent tanks, and c_3 the minimum clearance to the lower airfoil surface. The forward position of the outermost tank is determined by a user-defined offset from the leading edge. At this longitudinal location, the available airfoil thickness governs the maximum feasible tank diameter while satisfying the vertical clearance constraints. To maximize volumetric efficiency, each tank features a cylindrical main body followed by a conical aft section. The taper begins at the longitudinal position where either the upper or lower clearance limit becomes critical. The tank terminates when a user-defined minimum diameter of the conical section is reached, which simultaneously ensures compliance with the vertical clearance requirements and defines the overall tank length. Additional tanks are placed laterally as long as the resulting tank diameter remains above the specified minimum value.

In the aft tank layout (see Fig. 1b), the LH_2 tanks are positioned behind the rear cabin bulkhead and extend across the full width of the inner wing. Integration of the tanks requires an enlargement of the unpressurized aft segment. This is accomplished by increasing the height of the rear bulkhead, which, while maintaining a fixed cabin length, results in a taller and longer unpressurized aft segment. A scalar root-finding procedure is used to determine the minimum required bulkhead height at the cabin station that provides sufficient space for the tanks. In contrast to the lateral tank layout,

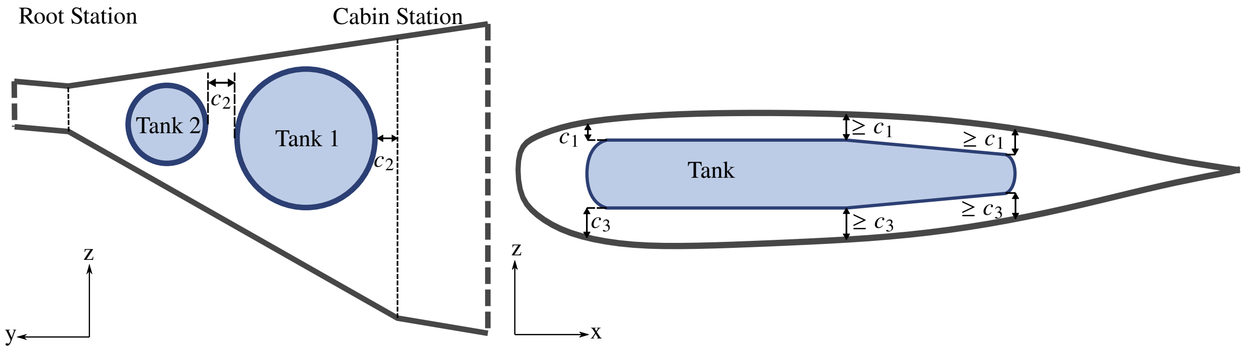

(a) Front-view. **(b) Side-view.**

Fig. 8 Lateral tank layout.

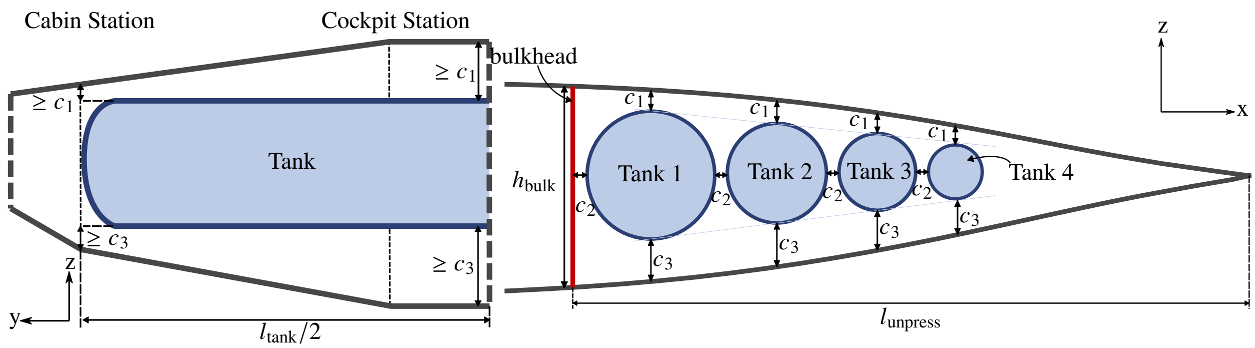

(a) Front-view. **(b) Side-view.**

Fig. 9 Aft tank layout.

the wing planform is not explicitly updated during this step. Instead, planform adaptation occurs implicitly through convergence within the overall aircraft design loop. The computed bulkhead height is transferred to the design tool openAD, which adjusts the rear bulkhead geometry and associated planform parameters to satisfy the imposed cabin height constraint. As illustrated in Fig. 9, the same clearance definitions as in the lateral tank layout are applied. The longitudinal reference position is corresponding to the rear cabin bulkhead location. The tanks are arranged sequentially in the aft direction, with the index n increasing downstream, each index representing one tank. Additional tanks are added successively until the resulting tank diameter falls below the specified minimum value.

The combined tank layout, visualized in Fig. 1c, utilizes both sizing approaches introduced for the lateral and aft tank layouts. In addition to the individual sizing parameters, the user defines a fuel distribution ratio between the two tank positions. The approach first sizes the lateral tanks, then passes the approximated planform to the aft tank approach for subsequent sizing. Resizing of the BWB is performed by passing the new cabin length-to-width ratio as well as the bulkhead height to openAD.

For the center tank layout, visualized in Fig. 1d, two tanks are arranged along the centerline of the BWB configuration. The aft tank includes a conical segment, the length of which is defined as a fraction of the centerline chord. Its end position is determined either by the location of the bulkhead or by a minimum allowable diameter of the conical segment. The diameter of the cylindrical portion is set to the maximum feasible value, based on the airfoil thickness at both the start of the conical segment and the front of the tank, and the required clearance. The clearances for the center tank layout are defined in Fig. 10. The second tank is positioned at a user-defined x-offset c_4 relative to the aft tank to allow for system integration. Its diameter is determined based on the maximum feasible value at the front and end of the tank. To meet regulatory requirements, this study assumes that the LH_2 tanks must be located outside of the pressure cell. To account for the additional mass from the added bulkheads, the mass of the wing area containing the center tanks is estimated using the cabin mass method. For this purpose, the area required for the LH_2 tanks is calculated, including

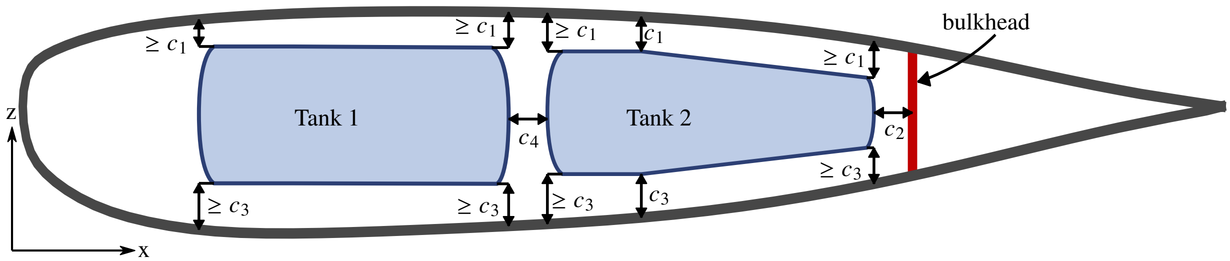

Fig. 10 Side-view center tank layout.

an offset from the cabin equal to the minimum required distance between tanks (c_2), which provides the necessary structural clearance. Aircraft resizing and mass estimation are then carried out by adding the total area occupied by the tanks to the area allocated for passenger accommodation and passing this combined area to openAD.

III. Reference and Baseline Aircraft Configurations

This study investigates a hydrogen-powered BWB designed to fulfill the requirements of a SMR mission. The Airbus A321neo is selected as the SMR reference aircraft to establish a consistent performance benchmark and is established using publicly available data [39]. The corresponding TLARs for this configuration are summarized in Table 1.

To enable a meaningful assessment of the derivative designs, it is essential to compare them against configurations that reflect an equivalent technological level [41]. This ensures that anticipated advancements in aerodynamics, propulsion systems, and structures are consistently applied to enable a sound evaluation of the relative performance implications of implementing LH_2 . Accordingly, a baseline design is developed from the selected reference aircraft, incorporating projected technological improvements for the assumed EIS year. Since the next generation of commercial aircraft is unlikely to adopt LH_2 as an energy carrier or introduce radical configurations such as the BWB, an EIS around 2050 is considered a realistic assumption. Separate baseline configurations are established for the conventional TAW aircraft and the BWB. The development of these derivative designs is described in the following.

Table 1 Top level aircraft requirements [40].

Parameter	Unit	Value
Design Range	nmi	2500
Design PAX (single class)	-	239
Mass per PAX	kg	95
Design Payload	kg	25000
Max. Payload	kg	25000
Cruise Mach number	-	0.78
Max. operating Mach number	kts	0.82
Maximum operating speed	kts	350
TOFL (ISA +0K SL)	m	2200
Rate of Climb @ TOC	ft/min	>300
Approach Speed (CAS)	kt	136
Wingspan gate limit	m	<36
Contingency	-	0.03

A. Tube-and-Wing Configurations

To provide a benchmark, the DLR developed a TAW research baseline aircraft designated DLR-F25, assuming an EIS in 2035. This configuration was introduced by Wöhler et al. [40] and serves as a technology-updated evolution of the reference aircraft. Key enabling technologies include an ultra-high bypass ratio (UHBR) propulsion system, a CFRP wing featuring folding wingtips, advanced load alleviation, and active flutter suppression.

To align with the assumed EIS of the BWB in the year 2050, the technology factors were re-evaluated accordingly. These updated factors build upon the DLR-F25, incorporating either incremental improvements or new technologies expected to be available by 2050. The applied factors for the TAW configuration with a 2050 EIS, relative to the DLR interpretation of the Airbus A321neo, are detailed and justified in Table 2. Compared to the DLR-F25, incremental improvements are assumed in engine performance, and in the mass of the wing and empennage. For the fuselage, a windowless CFRP design is assumed, reducing fuselage mass by an additional 10 % [42]. The application of riblet skin to the fuselage reduces the zero-lift drag by 2 % [43] and a wireless flight control system further reduces the system mass by an additional 2 % [42].

Table 2 Technology factors for the TAW baseline with EIS in 2050 relative to the DLR interpretation of the Airbus A321neo.

Component	Technology Factor	Rationale
Engine Performance	10 %	Compared to a 2015 state-of-the-art geared turbo fan: bypass-ratio 15, improved thermal efficiency, increased TET, incremental improvements.
Fuselage Mass	-15 %	Compared to D239: advanced CFRP structure with lower safety margin, improved manufacturing and assembly methods, but also revised production and certification requirements & windowless cabin.
Empennage Mass	-5 %	Compared to D239: advanced manufacturing and assembly methods.
Wing Mass	-35 %	Compared to D239: application of CFRP with lower safety margins, advanced load alleviation, active flutter suppression, adaptive dropped hinge flaps, and foldable wing tips.
System Mass	-7 %	Detailed system design performed for DLR-F25 [24] & wireless flight control.
Furnishing Mass	0 %	Potential mass reductions are mitigated by new requirements and certification rules as well as additional modularity, manufacturability, and increased complexity.
Operator Items Mass	0 %	Potential mass reductions are mitigated by new requirements and certification rules as well as additional modularity, manufacturability, and increased complexity.
Zero-Lift-Drag	-2 %	Riblet skin.

B. Blended Wing Body Configurations

For the BWB configurations, the same approach is chosen by starting the design process with an established reference aircraft from literature. The kerosene-fueled BWB introduced by Ahuja et al. [44], referred to as the reference BWB, was chosen. This aircraft, which is inspired by the JetZero BWB [20], represents a 2030 technology level and was chosen for its comparable size and the availability of detailed aerodynamic and mass data. Ahuja et al. [44] performed high-fidelity computer fluid dynamics (CFD) simulations of the configuration, enabling the calibration of the low-fidelity aerodynamic methods used in this study. The mass estimation is performed using NASA‘s Flight Optimization System (FLOPS).

To establish a BWB baseline consistent with the assumed 2050 EIS and aligned with the TLARs of the DLR-F25, an intermediate development step was introduced. The objective is to keep assumptions, methodologies, and calibration strategies as consistent as reasonably possible with those applied to the TAW baseline, thereby enabling a sound comparison. This intermediate configuration reflects a 2035 technology level and applies the DLR-F25 calibration factors to all analysis methods common to both TAW and BWB. Methods specific to the BWB, particularly in aerodynamics and

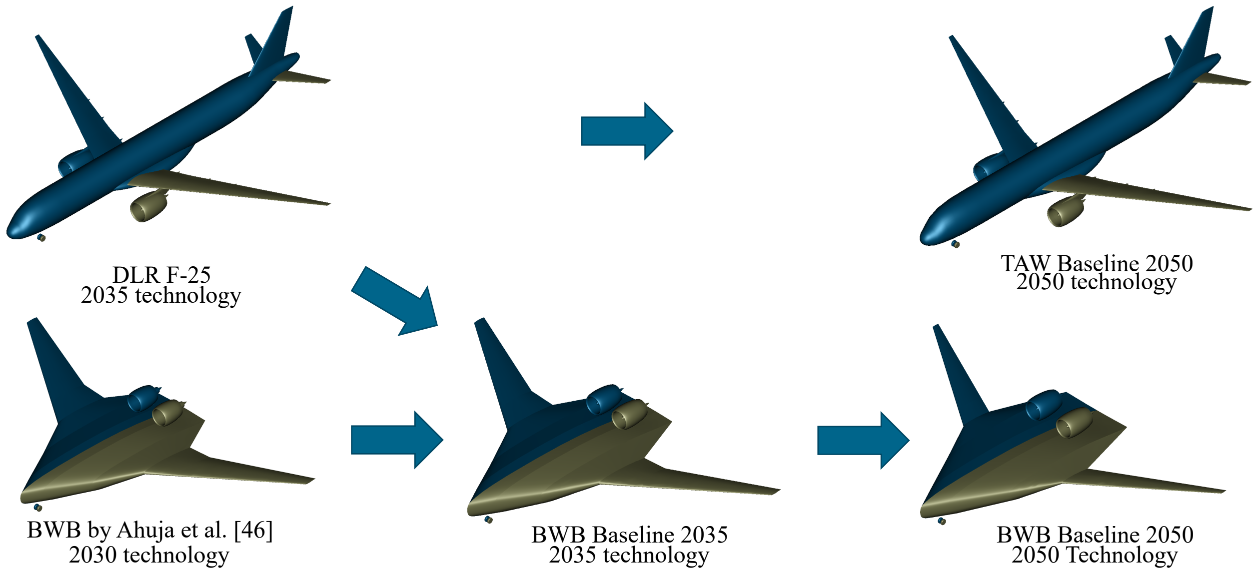

Fig. 11 Derivation of TAW and BWB baseline at 2050 technology level based on DLR-F25 and reference BWB.

structural mass estimation, are calibrated against the reference BWB configuration. The overall development process of the BWB baseline is illustrated in Fig. 11.

For the design of the BWB baseline with EIS in 2050, several assumptions and adaptions to the reference BWB are introduced. Since the airfoils of the reference BWB are not publicly available, airfoils from the VELA project [8] are employed, applying reflected airfoils to the inner wing and supercritical airfoils to the outer wing. For the maximum take-off and landing lift coefficient, the value of approximately 1.0 reported by Kawai [45] for a BWB with drooped leading-edge slats using the same airfoils as Ahuja et al. [44] is adopted.

The planform of the BWB is derived from the configuration presented by Ahuja et al. [44], with targeted modifications to ensure consistency with the DLR-F25 requirements. For the present study, the cabin is resized to match the passenger density of the DLR-F25. A 10 % increase in cabin area is applied to account for the less efficient space utilization inherent to the BWB compared to a conventional TAW layout, as well as the geometric idealization of the cabin extending to the wing leading edge (see Chapter II). The transition wing width is fixed at 13 % of the semi-span, consistent with the reference configuration.

Regarding cargo integration, most BWB concepts accommodate freight either within the transition wing or beneath the cabin. For the present baseline, the available volume below the cabin proved insufficient for meaningful cargo storage. Consequently, cargo is allocated to the unpressurized transition wing. While this arrangement introduces operational constraints compared to the TAW configuration it is assumed that these limitations can be operationally managed. A small pressurized bulk compartment beneath the cabin is considered for pressure-sensitive goods or live animals.

For the reference BWB, the framework predicts a mid-cruise static margin of -13 %, indicating a statically unstable configuration. Given the limited fidelity of the applied assessment methods and the fact that geometrically similar BWB concepts reported in the literature [8, 46] exhibit positive static margins, this value is adopted as a practical design target rather than an absolute result. After resizing the configuration for the BWB baseline, a further reduction in static margin was observed. To compensate, the layout was adjusted by repositioning the outer wing further aft and outboard, restoring the mid-cruise static margin to approximately the reference level. Although increasing the inner wing leading-edge sweep could also improve static stability, this option was not pursued due to potential drawbacks in low-speed performance associated with highly swept wings.

Technology factors are also applied to the baseline BWB configuration. For all common components, the same factors as for the TAW baseline are adopted. However, due to the fundamentally different structural layout of the BWB, the conventional wing, fuselage, and empennage are replaced by the pressurized passenger segment, the unpressurized aft segment, and the transition and outer wing, which are treated separately. It should be noted that the reference BWB already incorporates technology assumptions corresponding to approximately a 2030 EIS. Consequently, the additional technology factors applied in this study are defined relative to the BWB presented by Ahuja et al. [44],

Table 3 Technology factors for the BWB baseline with EIS in 2050.

Component	Technology Factor	Rationale
Pressurized Segment Mass	-27 %	PRSEUS [44].
Unpressurized Segment Mass	-23 %	PRSEUS [44].
Outer Wing Mass	-35 %	Advanced load alleviation, active flutter suppression, adaptive dropped hinge flaps, and foldable wing tips. Application of CFRP with lower safety margins.
Transition Wing Mass	-15 %	Application of CFRP [44].

Table 4 LH_2 tank design parameters.

Parameter	Unit	Value	Remark
Unusable fuel	%	10	w.r.t. max. fuel mass [48]
Ullage volume	%	5	w.r.t. tank volume [49]
Insulation thickness	m	0.05	Vacuum spacing [48]
Maximum pressure	bar(a)	2.5	Structural sizing condition [50]
Factor crash structure	-	0.03	Factor on total tank mass
Factor mount structure	-	0.04	Factor on total tank mass

ensuring consistency.

The complete set of technology factors applied to the 2050 baseline Blended Wing Body is summarized in Table 3. For the pressurized passenger segment and the unpressurized aft segment, the BWB baseline adopts the PRSEUS structural concept [47]. The associated mass reductions are taken from Ahuja et al. [44], who provide a detailed comparison between PRSEUS and conventional CFRP structures. For the outer wing at a 2035 EIS, the same technology assumptions as for the DLR-F25 are applied. Since the reference BWB already includes a 15 % mass reduction due to the use of CFRP, this benefit is accounted for when applying additional factors. For the 2050 EIS, PRSEUS-related mass savings are conservatively held constant, reflecting uncertainties regarding its large-scale industrial implementation beyond the early 2030s. A similar approach is taken for the transition wing, for which only the 15 % CFRP-related mass reduction is assumed.

IV. Liquid Hydrogen Integration

Building on the kerosene baseline designs, LH_2 is systematically integrated as an energy carrier. A LH_2 TAW configuration is developed alongside four LH_2 BWB concepts, as illustrated in Fig. 1. This chapter presents the overarching assumptions governing LH_2 integration for both configurations and describes the design philosophy specific to each concept.

A. Global Assumptions

A consistent set of global assumptions is applied to the tank design for both the TAW and BWB configurations (Table 4). These parameters define the volumetric margins, structural sizing conditions, and mass allowances used throughout the study. The ullage requirement and unusable fuel fraction account for operational constraints, while the maximum tank pressure represents the governing structural sizing case. In addition, structural mass allowances for crash and mounting provisions are incorporated based on expert judgment at DLR.

At aircraft level, the technology factors applied to the LH_2 configurations are summarized in Table 5. These factors represent the primary performance and structural effects associated with hydrogen integration. The propulsion efficiency adjustment [51] reflects thermodynamic differences in hydrogen combustion, while the wing-mass penalty accounts for the absence of fuel load relief in dry-wing configurations [50]. Although the BWB features a reduced outer wingspan and therefore potentially lower bending moments, this structural advantage has not been quantified and is consequently

Table 5 Technology assumptions for the LH_2 aircraft configurations.

Component	Value	Rationale
Engine Performance	3.6 %	Compared to a 2035 state-of-the-art geared turbo fan, higher specific heat capacity in exhaust mass flow [51].
(Outer) Wing Mass	5.0 %	No relief of wing structure due to dry wing [50].
LH_2 System	730 kg	Additional mass based on a component mass breakdown method from Brewer [3].

not credited in the present analysis. In addition, a dedicated LH_2 system mass is included. Rather than performing a detailed bottom-up estimation, a fixed system mass derived from a prior component-level breakdown study is applied at the tanks' weighted center of gravity [3, 50]. This mass is assumed to be identical for both TAW and BWB configurations, as the impact of the BWB layout on system mass cannot be reliably quantified within the scope of this work.

B. Tube-and-Wing Configuration

The LH_2 TAW configuration builds on the hydrogen combustion aircraft developed by Kotzem et al. [50], which itself is derived from the DLR-F25. For the present study, the design is updated to a 2050 technology level using the technology factors given in Table 2, while maintaining the same TLAR as the corresponding kerosene baseline to ensure comparability.

Two cylindrical LH_2 tanks are integrated aft of the rear pressure bulkhead, necessitating an increase in fuselage length and/or diameter. A trade study on seats-abreast configurations identified a twin-aisle layout with eight seats abreast as the most energy-efficient solution that still ensures ground-handling access to the rear doors, thereby limiting the required fuselage extension. The increased fuselage diameter reduces the available wingspan for high-lift devices, leading to a decrease in the maximum landing lift coefficient. In addition, the maximum take-off lift coefficient is intentionally reduced to enforce a higher take-off speed, increasing the dynamic pressure at the horizontal tail plane (HTP) and thereby enabling a smaller tail size. As engine thrust is governed by the top-of-climb requirement, these modifications do not result in an increase in engine mass.

The configuration is further refined within the Clean Aviation ACAP project [52], by replacing the conventional tail with a T-tail arrangement. A conventional layout would require an extended empennage to accommodate the HTP intersecting the fuselage, whereas the T-tail avoids this intrusion and allows for a shorter empennage, improving overall performance. Consistent with the underlying design by Kotzem et al. [50], a clearance of 0.5 m is maintained below the tank to accommodate a crash structure, 0.2 m above for integration with the surrounding fuselage, and 1.5 m between tanks to allow for LH_2 system integration.

C. Blended Wing Body Configuration

The LH_2 integration into the BWB configuration follows the tank layouts identified from literature [10–17, 21]. These four tank layouts are therefore developed from the kerosene BWB baseline under identical TLAR: a lateral layout with tanks positioned beside the passenger cabin, an aft layout with tanks located behind the cabin, a combined layout incorporating both lateral and aft tanks, and a centerline layout with tanks arranged along the aircraft symmetry plane (see Fig. 1).

The outer wing geometry is preserved to maintain comparability with the kerosene baseline. A minimum outer wing aspect ratio equal to that of the reference aircraft is enforced, and the wingspan is fixed at 45 m. Sensitivity to this assumption is examined separately in chapter V.C. To comply with the 36 m gate limit specified in the TLAR, folding wingtips are incorporated.

A key design parameter is the static margin of the BWB, which is directly influenced by the outer wing position. The outer wing position is determined by the inner wing leading-edge sweep and the lateral position of the outer wing root. However, in this study, the inner wing leading-edge sweep is held constant due to its potential impact on low-speed performance.

For the TAW configuration, clearances are defined both between adjacent LH_2 tanks and between tanks and the surrounding structure. These clearances are reassessed for the BWB configuration. In the TAW layout, clearances are prescribed as constant values along the entire tank length. In contrast, for the BWB they are interpreted as minimum required clearances, allowing local geometric adaptation to the airframe. Furthermore, due to their smaller diameters, the BWB tanks distribute the same hydrogen volume over a larger surface area. This reduces the load per unit area in crash scenarios and justifies a reduction of the crash-structure clearance c_3 to 0.35 m. Regarding system integration, no additional dedicated clearance is allocated in the lateral, aft, and combined tank layouts, as the tanks are arranged side-by-side. Instead, LH_2 subsystems are assumed to be installed at the tank end domes or within the residual gaps between tanks and primary structure. These spaces remain available because structural packing within the BWB center body is less constrained than in the TAW fuselage. A tank-to-tank clearance c_2 of 0.10 m is maintained to accommodate suspension and structural interfaces. For the center tank layout, a longitudinal tank-to-tank clearance c_4 of 0.5 m is specified. This provides additional integration volume at the tank domes while still taking advantage of the comparatively generous internal space of the BWB. Finally, for the lateral and combined layouts, the minimum conical-segment diameter of the lateral tanks is set to d_{con} = 0.6 m to ensure geometric feasibility and structural continuity.

V. Results

This chapter presents the results for the BWB configurations with integrated LH_2 as energy carrier, based on the assumptions and design philosophies established in the preceding chapters. A systematic downselection process is conducted to identify the tank layout that minimizes integration penalties within the BWB configuration. This selected configuration then serves as the basis for a direct comparison with the corresponding TAW layout.

The analysis quantifies the relative performance impacts of LH_2 integration for both BWB and TAW concepts and evaluates sensitivities to key design assumptions across the different tank arrangements. Finally, the results are consolidated into a set of derived design principles to guide future BWB aircraft development with integrated LH_2 storage.

A. Blended Wing Body Downselection

A systematic downselection is conducted to identify the LH_2 tank layout that results in the lowest overall integration penalty. For this purpose, a dedicated aircraft design is developed for each tank layout. The primary objective of this study is to quantify the integration penalties associated with LH_2 relative to the corresponding kerosene configuration. Therefore, all results presented in the following are expressed relative to the kerosene BWB baseline introduced in Chapter III, ensuring a consistent reference framework for comparison.

Figure 12 shows key performance parameters of the BWB for the lateral, aft, and center tank layout. For this, the lateral position of the wing root position is varied to investigate the effects on the static margin, the gravimetric efficiency, the block energy and OEM.

The static margin results shown in Fig. 12a indicate that moving the wing root further outboard increases the static margin for all configurations. This trend is caused by the aft shift of the quarter-chord point of the mean aerodynamic chord (MAC). The initial objective was to maintain approximately the same mid-cruise static margin as the kerosene baseline. However, the results show that achieving this target would require modifications to additional planform parameters, which were intentionally kept fixed to preserve aerodynamic comparability to the reference BWB. Consequently, the original static margin requirement was relaxed, and a secondary requirement was introduced for the LH_2 configurations. This revised requirement was set to a static margin of -0.16, representing a value close to the reference BWB that could be consistently achieved across all configurations while maintaining comparability.

The gravimetric efficiency is shown in Fig. 12b. The center layout achieves by far the highest gravimetric efficiency, reaching approximately 45 % across all root positions and exhibiting almost no sensitivity to the wing root location. This behavior results from the large wing thickness at the centerline, which allows for the largest tank diameters and, consequently, the lowest tank aspect ratios. For the lateral tank layout, the gravimetric efficiency remains nearly constant over most root positions, with the exception of a discrete change. This step occurs when the tank-fitting algorithm assigns an additional tank within the transition wing. At the three most inboard root positions, only one tank is accommodated in the transition wing. With this step, a second tank is introduced. Although this shortens the first tank, the smaller diameter of the added tank reduces the overall gravimetric efficiency. In the aft tank layout, the gravimetric efficiency decreases steadily as the wing root shifts outboard. This trend is explained by the increasing inner wingspan, which lengthens the tanks while reducing the available height required to house them. The resulting decrease in average tank diameter leads to the observed decline in gravimetric efficiency.

The relative change in block energy with respect to the BWB baseline is shown in Fig. 12c. An increase in block energy is observed, primarily driven by the reduction in gravimetric efficiency, which results in a higher tank mass for the same hydrogen mass. Furthermore, as the wing root is shifted outboard, the increase in inner and transition wing

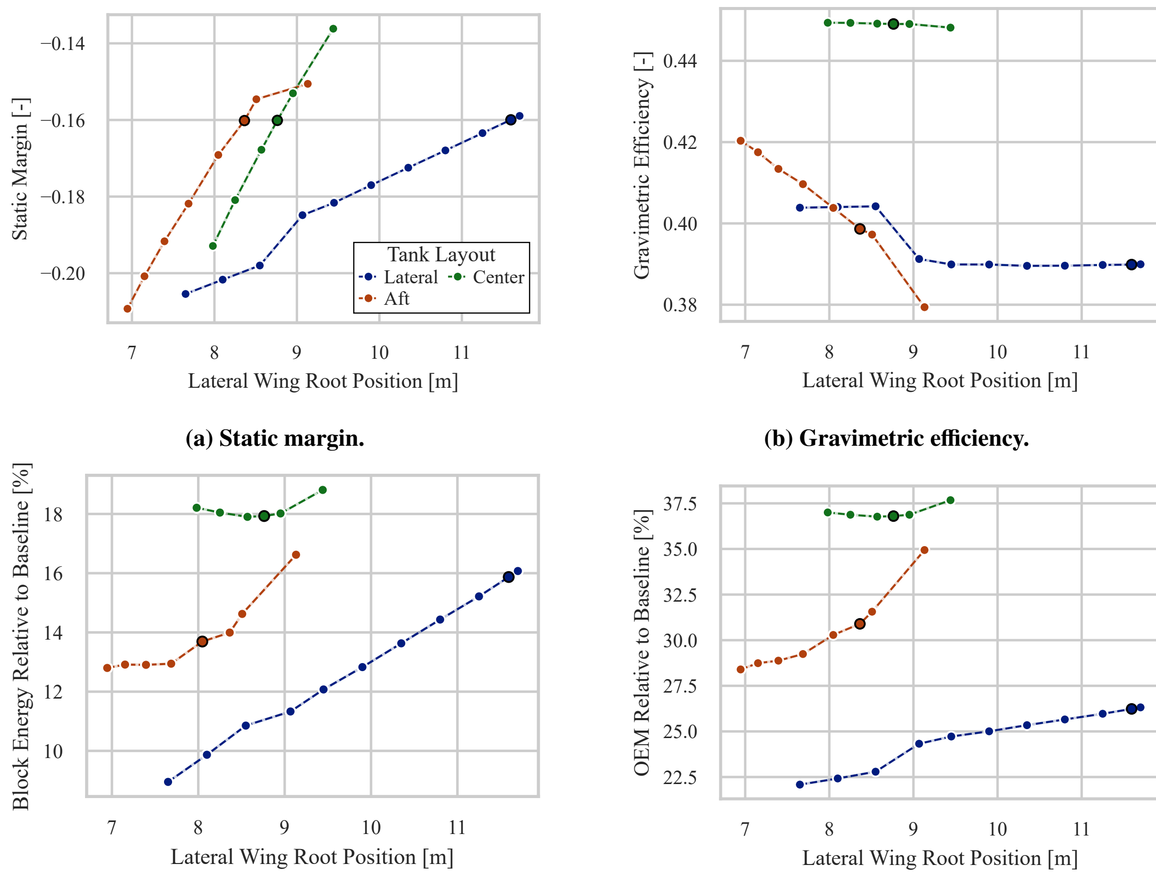

(a) Static margin.

(b) Gravimetric efficiency.

(c) Block energy.

(d) OEM.

Fig. 12 Key performance parameters of lateral, aft, and center tank layout for changing wing root position. Selected configurations highlighted by black outline.

area generally outweighs the decrease in outer wing area, resulting in a net growth in total wing area. This behavior occurs because both the unused portion of the unpressurized aft section and the tank-occupied area expand, while the outer wing area in most LH_2 configurations is determined by the aspect ratio constraint rather than by the landing field length requirement. Consequently, the total wing area, and thus the structural mass, increases. Finally, increasing the wing area while maintaining a constant wingspan reduces the overall aspect ratio, leading to higher induced drag and further contributing to the rise in block energy.

The changes in OEM shown in Fig. 12d parallel the changes in block energy, with the aft tank layout experiencing a comparatively greater impact than the other configurations.

The combined tank layout is analyzed separately due to the trade-off between the fuel fraction allocated to the lateral tanks and that stored in the aft tanks. Figure 13 presents the key performance parameters for fuel mass fractions ranging from 20 % to 80 % in the lateral tanks, with the remainder assigned to the aft tanks.

Overall, trends similar to those observed for the other tank layouts in Fig. 12 can be identified, regarding the influence of static margin and gravimetric efficiency on block energy and OEM. The variation in gravimetric efficiency, in particular, reflects a superposition of the tendencies observed in the individual lateral and aft layouts. The gradual decrease with increasingly wing root positions is mainly driven by the reduction in aft tank diameter, whereas the discrete increase is associated with the introduction of a second lateral tank.

For the combined tank layout, Fig. 14 presents the block energy requirement and OEM as a function of the lateral fuel mass fraction at a static margin of -0.16. A value of 0 corresponds to the pure aft tank layout, while a value of 1 represents the pure lateral tank layout. This representation enables the identification of the lateral fuel mass fraction and corresponding root position that minimize the block energy requirement. A certain degree of irregularity in the

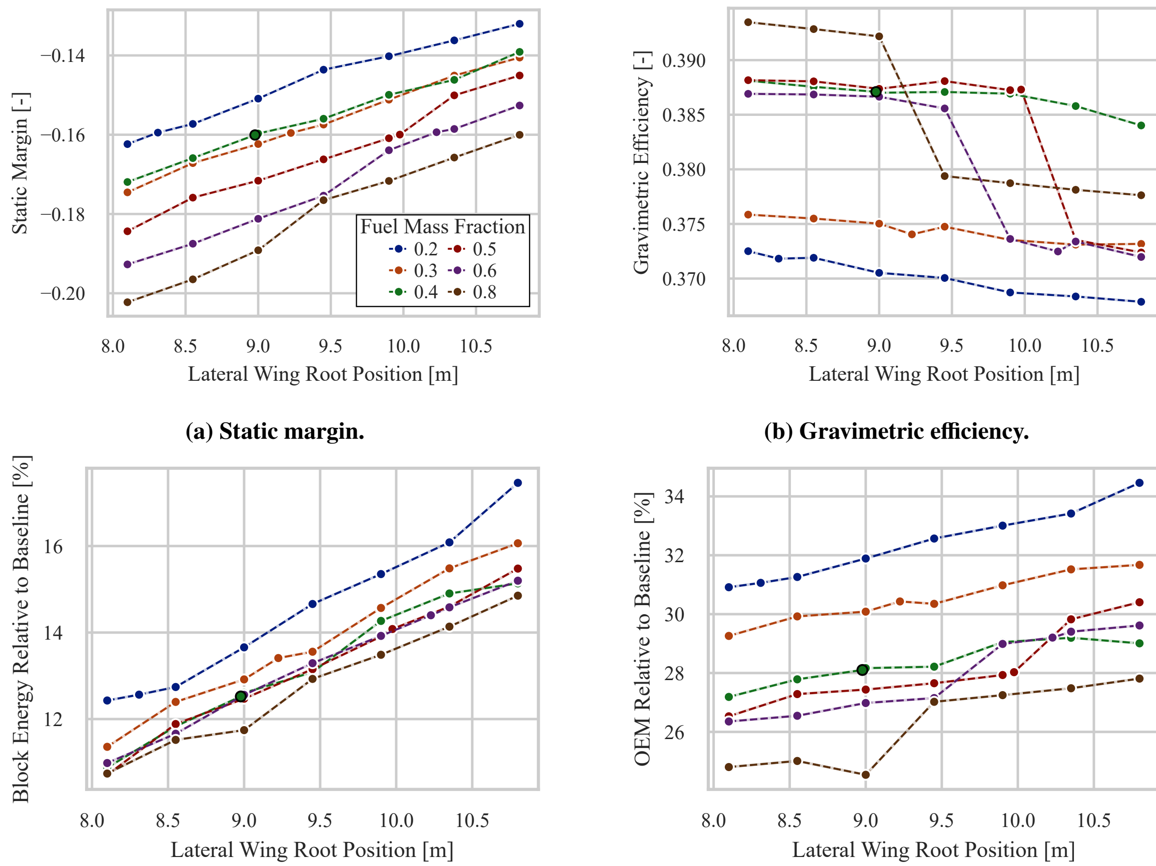

(a) Static margin.

(b) Gravimetric efficiency.

(c) Block energy.

(d) OEM.

Fig. 13 Key performance parameters of combined tank layout for changing wing root position and lateral fuel mass fraction. Selected configuration highlighted by black outline.

variation of block energy and OEM with increasing lateral fuel mass fraction can be observed. These fluctuations are attributed to discontinuities in the tank integration process and the absence of a dedicated optimization of the tank layout. Consequently, some configurations store hydrogen more efficiently than others, leading to deviations from a strictly continuous trend.

Based on the static margin criterion of -0.16 and the objective of minimizing block energy consumption, one configuration per tank layout was selected. These selected configurations are highlighted with a black outline. For the combined tank layout, the optimal configuration corresponds to a lateral fuel mass fraction of 40 % and a wing root position at 40 % of the wingspan. For these configurations, Fig. 15 summarizes the impact of LH_2 integration on the BWB relative to the kerosene baseline in terms of key performance parameters. All hydrogen-fueled configurations exhibit increases in block energy consumption, MTOM, and OEM, accompanied by a reduction in lift-to-drag ratio. Although the lateral tank layout yields the lowest OEM, this advantage is offset by its comparatively poor aerodynamic performance, making the combined and aft tank layout more favorable overall. Among the LH_2 concepts, the combined tank layout results in the lowest block energy requirement, whereas the center tank layout shows the highest. Based on these findings, the combined tank layout is selected for further comparison.

B. Comparison of Blended Wing Body and Tube-and-Wing Configurations

A comparative assessment is conducted between the selected LH_2 -fueled BWB configuration, the kerosene-fueled BWB baseline, and the conventional TAW aircraft operated with both LH_2 and kerosene, in order to quantify the relative effects of fuel type and aircraft configuration.

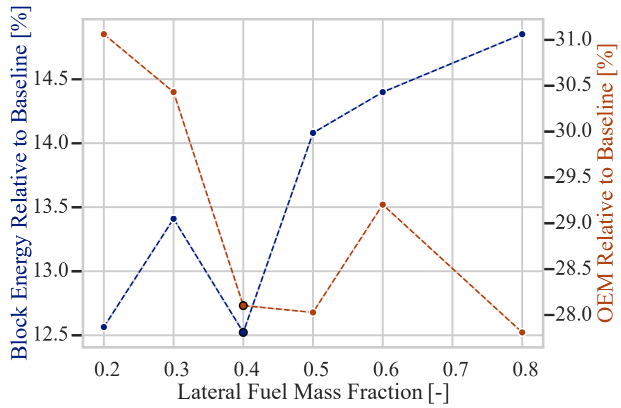

Fig. 14 Block energy and OEM as a function of lateral fuel mass fraction for a static margin of -0.16. Selected configuration highlighted by black outline.

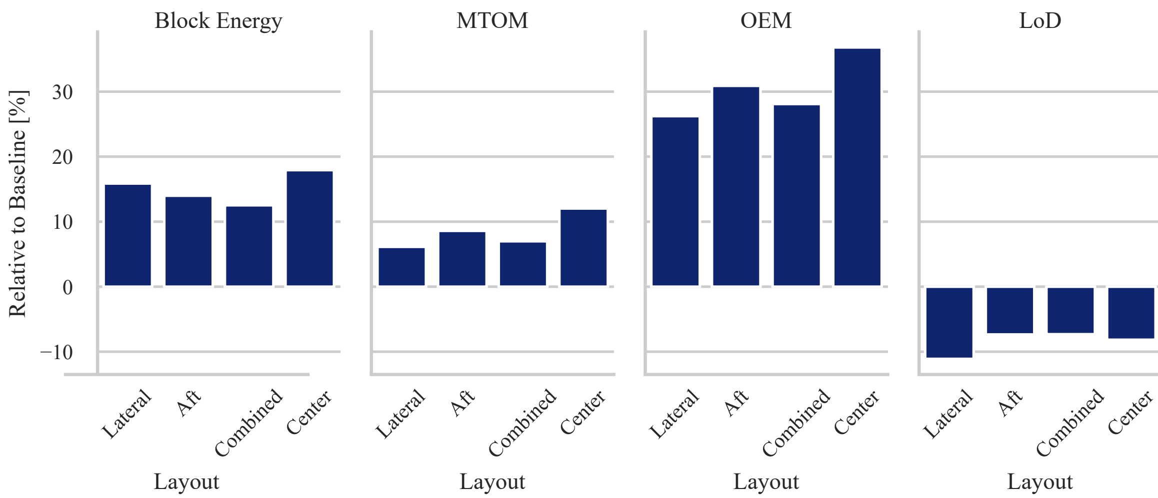

Fig. 15 Comparison of aircraft performance metrics for selected BWB configurations.

Performance Characteristics

Table 6 summarizes the performance characteristics of these configurations. The primary outcome of this comparison concerns differences in fuel mass and energy requirements. Relative to the kerosene baseline, both the TAW and BWB LH_2 configurations achieve an approximately 60 % reduction in block fuel mass, reflecting the higher specific energy of LH_2 . However, this reduction in fuel mass is accompanied by an increase in energy consumption: the LH_2 TAW requires 10.5 % more block energy than its kerosene counterpart, while the LH_2 BWB exhibits a 12.5 % increase in block energy. Overall, the LH_2 integration penalty for the BWB on the design mission is 2.0 % higher than for the TAW.

The underlying design effects leading to this result can be summarized as follows:

- The LH_2 variants of the TAW and BWB exhibit reductions in wing loading of 10.9 % and 12.0 %, respectively. For the TAW, this reduction primarily results from a lower fuel fraction, which increases maximum landing mass (MLM) relative to MTOM and thus drives wing sizing. In the BWB case, although the fuel fraction effect is similar, the decrease in wing loading is mainly driven by the increase in inner wing area required for tank integration, leading to a larger total wing area, while the outer wing remains constrained by the aspect ratio requirement.
- For the TAW configuration, LH_2 integration leads to a higher thrust-to-weight ratio, mainly as a consequence of the reduced wing loading and the resulting top-of-climb thrust requirement. In contrast, the BWB shows a negligible decrease in thrust-to-weight ratio.
- In both configurations, the increased wing area at constant wingspan results in a reduction in aspect ratio. The

Table 6 Comparison of LH_2 TAW and BWB configurations against respective TAW and BWB kerosene baselines.

Parameter	Unit	TAW			BWB		
		Kerosene	LH2	Delta	Kerosene	LH2	Delta
Wing Loading and Thrust-to-Weight Ratio							
W/S = MTOM / Wing Ref. Area	kg/m^2	652.52	581.11	-10.9 %	225.95	198.94	-12.0 %
T/W = SLST / MTOM	-	0.294	0.316	7.6 %	0.323	0.322	-0.2 %
Masses							
MTOM	t	81.51	84.64	3.8 %	80.98	86.63	7.0 %
MLM	t	71.17	80.53	13.1 %	71.81	82.94	15.5 %
MZFM	t	68.57	79.49	15.9 %	69.50	82.01	18.0 %
OEM	t	43.57	54.48	25.0 %	44.50	57.01	28.1 %
Wing Geometry							
Wingspan	m	45	45	0.0 %	45	45	0.0 %
Wing Aspect Ratio	-	16.21	13.90	-14.2 %	5.65	4.65	-17.7 %
Wing MAC	m	3.40	3.94	%15.9 %	17.28	21.29	23.2 %
Wing Ref. Area	m^2	124.92	145.65	16.6 %	358.38	435.48	21.5 %
Aerodynamics							
Lift-to-drag-ratio (avg. Cruise)	-	20.15	18.83	-6.5 %	23.54	21.82	-7.3 %
Lift Coefficient (avg. Cruise)	-	0.60	0.60	-0.2 %	0.31	0.29	-7.9 %
Max. Lift Coefficient (Landing)	-	2.85	2.76	-3.0 %	1.00	1.00	0.0 %
Design Mission (Range = 2500 nmi and Payload = 25000 t)							
Block Fuel	t	10.84	4.31	-60.2 %	9.48	3.84	-59.5 %
Block Energy	GJ	468.32	517.61	10.5 %	409.85	461.17	12.5 %

impact of LH_2 integration on aspect ratio, MAC, and reference area is slightly more pronounced for the BWB than for the TAW. Consequently, both configurations experience a degradation in aerodynamic efficiency, which is slightly more significant for the BWB.

Table 6 also enables a direct comparison between the TAW and BWB concepts. This comparison should, however, be interpreted with caution due to differences in underlying methods and assumptions. The kerosene-fueled BWB exhibits approximately 12.5 % lower block energy consumption than the kerosene TAW. While the BWB shows a slightly higher OEM and a comparable MTOM, it achieves a substantially higher mid-cruise lift-to-drag ratio of 23.5, compared to 20.2 for the TAW. For the LH_2 variants, the BWB demonstrates a 10.9 % lower block energy requirement than the LH_2 TAW.

Planform Comparison

Figure 16 compares, the planforms of the kerosene (bottom) and LH_2 (top) configurations for the TAW and BWB configurations. For the TAW configuration, the LH_2 configuration exhibits a larger fuselage diameter and an extended fuselage length relative to the kerosene baseline. In the BWB configuration, a similar increase in inner wing length can be seen, accompanied by the outer wing moving outboard and aft. The unused area in the transition wing of the LH_2 BWB is approximately equal to the transition wing area in the kerosene configuration, indicating that an increase in transition wing area is always required to accommodate any LH_2 tanks. Comparing the TAW and BWB configurations, it becomes apparent that the BWB is much shorter than the TAW.

Table 7 provides a breakdown of the tanks employed in the selected BWB and TAW configurations, respectively. The gravimetric efficiency is shown both including unusable fuel, as defined in Eq. (4), and excluding unusable fuel. This is done to increase comparability since some studies do not include unusable fuel in the gravimetric efficiency. The unusable fuel, comprising pressurization fuel mass and trapped fuel mass, reduces gravimetric efficiency by approximately 2 to 4 %, with a greater impact observed at higher gravimetric efficiencies. This increased impact can be attributed to the unusable fuel remaining constant for a given total fuel mass, while its proportion of the total tank mass increases as the structural tank mass decreases.

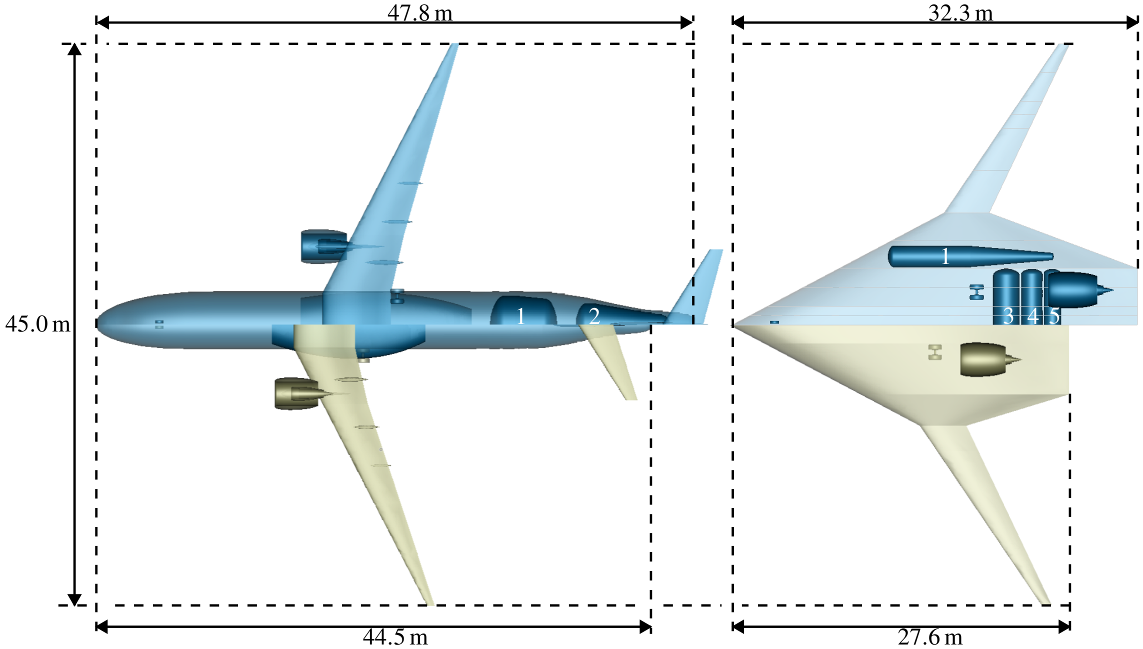

(a) TAW configuration. **(b) BWB configuration.**

Fig. 16 Planform comparison of kerosene (bottom) and LH_2 (top) configurations.

For the TAW, the difference in gravimetric efficiency between the two tanks is minimal, even though tank 1 stores approximately twice the amount of fuel as tank 2. In contrast, the BWB configuration exhibits much larger differences in gravimetric efficiency. Tanks 1 and 2, which correspond to the lateral tanks of the selected BWB (see Fig. 16b), have very low gravimetric efficiencies due to their high aspect ratio. In comparison, tanks 3 and 4, which store similar amounts of fuel but are located in the unpressurized aft segment, achieve noticeably higher gravimetric efficiencies. This highlights the importance of including the effect of the geometrical shape of the tank on the gravimetric efficiency.

Volumetric Efficiency

In addition to the gravimetric efficiency, another key metric is how effectively the additional volume required for LH_2 integration is utilized. This is captured by the volumetric efficiency, which describes how efficiently the available additional volume is used for LH_2 storage. As there is no universal definition, this paper defines the volumetric efficiency η_v as

$$\eta_v = \frac{v_{LH2}}{v_{A/C,\,LH2} - v_{A/C,\,kerosene}}, \tag{5}$$

where v_{LH2} is the volume of usable LH_2 , $v_{A/C,\,LH2}$ is the total volume of the hydrogen-fueled aircraft (including fuselage and wing for the TAW configuration), and $v_{A/C,\,kerosene}$ is the total volume of the kerosene-fueled baseline aircraft. At 0.24, the volumetric efficiency of the hydrogen-fueled BWB exceeds that of the TAW at 0.20, indicating that the BWB utilizes its available volume slightly more effectively. This difference can be partly explained by the larger diameter of the TAW configuration, which accommodates tank integration in the lateral direction but leads to increased unused space in the vertical direction. In addition, the BWB likely benefits from its greater thickness, which allows the cargo hold, previously located in the transition wing, to be repositioned beneath the cabin, thereby further improving volumetric efficiency.

C. Method Limitations and Sensitivity Studies

This study is based on several assumptions and methodological limitations, which are outlined below together with their potential impact on the results. Subsequently, the sensitivity on the results to selected key assumptions are assessed.

Table 7 **Mass breakdown of LH_2 tanks.**

Parameter	Unit	TAW			BWB				
		Tank 1	Tank 2	Total	Tank 1 & 2	Tank 3	Tank 4	Tank 5	Total
Tank Position	-	Aft	Aft	-	Lateral	Aft	Aft	Aft	-
Gravimetric Efficiency	-	0.45	0.44	0.45	0.37	0.42	0.39	0.35	0.39
Gravimetric Efficiency (Excl. Unusable Fuel)	-	0.48	0.48	0.48	0.40	0.45	0.42	0.37	0.41
Structural Masses									
Total Tank Mass	kg	3625	1940	5565	1417	1650	1203	911	6598
Vessel Mass	kg	3006	1614	4620	1219	1388	1026	790	5642
Crash Structure and Attachment Mass	kg	619	326	944	198	262	177	121	956
Fuel Masses									
Total Fuel Mass	kg	3983	2076	6059	1090	1609	1025	633	5446
Usable Fuel Mass	kg	3410	1777	5187	933	1377	877	542	4662
Pressurization Fuel Mass	kg	175	91	266	48	71	45	28	239
Trapped Fuel Mass	kg	398	208	606	109	161	102	63	545

- This study relies on low-fidelity mass-estimation methods that may not capture all sensitivities of LH_2 tank integration. For example, using the cabin-mass approach for estimation could unfairly penalize the center tank layout.
- This study does not consider a detailed structural layout. It assumes that the tank position is constrained only by structural clearances and not by other factors, such as wing spars, that could restrict LH_2 tank placement.
- For the hydrogen system integration on the BWB configuration, the same assumptions are made as for TAW LH_2 configurations. However, due to the larger number of tanks, the system mass could be significantly increased, which is not accounted for.
- The study relies on low-fidelity aerodynamic methods originally developed for conventional TAW aircraft. Although these methods are calibrated against high-fidelity data from a reference aircraft, they may not fully capture the aerodynamic characteristics and sensitivities of a BWB configuration. This limitation imposes two main constraints. First, design variations must be restricted to preserve comparability with the calibrated baseline. Second, certain aerodynamic effects specific to the BWB configuration may not be fully represented, potentially limiting the accuracy of the predicted performance trends.
- This study does not consider regulatory evacuation requirements. Such requirements may further constrain the cabin, planform, and tank layout due to limits on the maximum distance to emergency exits.

LH_2 Integration Assumptions

The sensitivity to tank mass is assessed by applying a structural LH_2 tank mass penalty ranging from -50 % to +100 % of the nominal value to all four BWB configurations and the TAW. This allows a direct comparison of their relative sensitivity. As shown in Fig. 17a, the combined tank layout is less sensitive to moderate tank mass increases than the TAW, partly due to its higher lift-to-drag ratio, which mitigates the impact of additional mass on energy consumption. Up to a penalty of about 40 %, the integration penalty of the BWB is comparable to that of the TAW. Beyond this threshold, however, the BWB becomes more sensitive. This behavior is linked to the BWB sizing approach. For penalties up to 40 %, wing area is constrained by the outer wing aspect ratio requirement, keeping wing area and wing mass nearly constant. For higher penalties, the landing field length requirement becomes sizing-critical. Because the BWB has a relatively low maximum landing lift coefficient (1.0 compared to 2.76 for the TAW), an equivalent increase in landing mass requires a significantly larger wing area increase, leading to a stronger mass growth that offsets the aerodynamic advantage. The general trend is consistent across the BWB configurations, except for the lateral tank layout, where the stronger rise in energy penalty at high mass penalties is not observed. Figure 17b compares the relative integration penalty as a function of gravimetric efficiency. For efficiencies below 0.46, the combined tank BWB shows a smaller relative performance penalty than the TAW. However, for a given tank technology, the BWB achieves a lower absolute gravimetric efficiency than the TAW.

For the BWB, lower clearances are applied between the tanks and the structure compared to the TAW configuration.

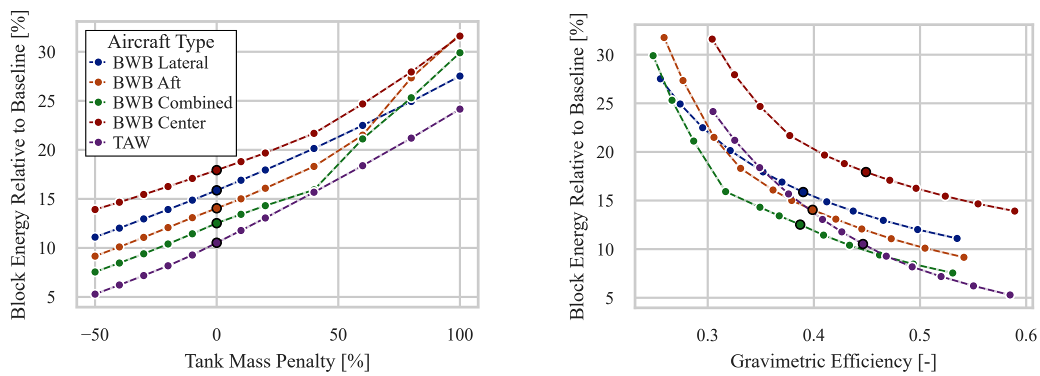

(a) Relative to tank mass penalty. **(b) Relative to gravimetric efficiency.**

Fig. 17 Sensitivity of LH_2 configurations to tank mass. Original configurations highlighted by black outline.

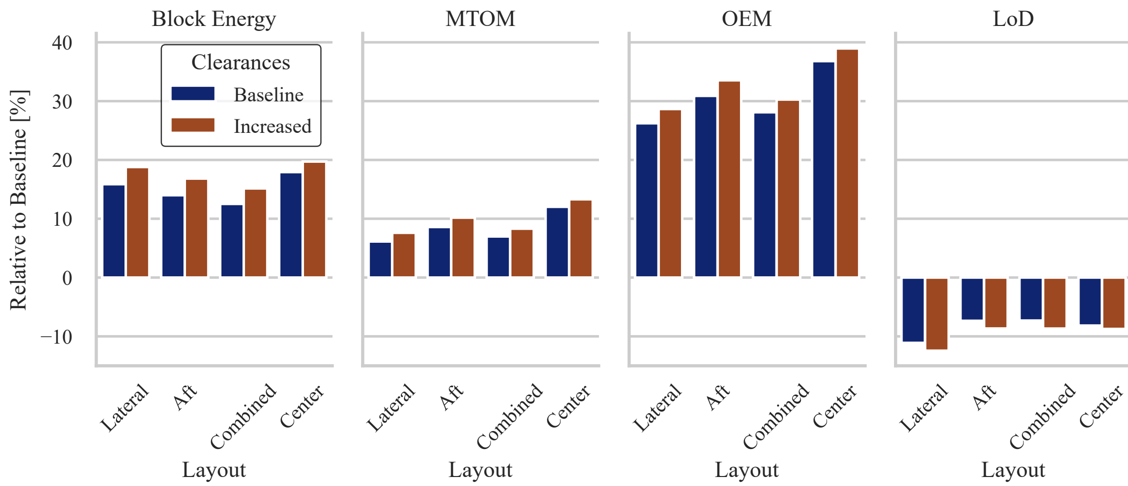

Fig. 18 Sensitivity of LH_2 configurations to clearances.

To evaluate the impact of this assumption, the clearances applied to the TAW (see Chapter IV.B) are applied to the BWB. The side-to-side clearance between tanks c_2 is increased to 0.2 m. Figure 18 shows the impact on key performance parameters. The resulting increase in block energy ranges from approximately 2 % to 3 %, with the greatest impact observed for the lateral tank layout and the lowest for the center tank layout. However, this does not alter the relative favorability of the different configurations.

For the four LH_2 BWB configurations, the outer wing is sized to satisfy the aspect ratio requirement. This constraint can be fulfilled either by increasing the outer wing area at constant wingspan or by reducing the wingspan while maintaining a constant outer wing aspect ratio. In this study, the wingspan is fixed and the outer wing area is increased. To evaluate the impact of this assumption, Fig. 19 compares configurations with fixed and flexible wingspans. For the flexible-span cases, the resulting wingspans are 41.65 m (aft tank layout), 41.05 m (combined tank layout), and 42.71 m (center tank layout). Although reducing the wingspan while maintaining the outer wing aspect ratio should theoretically decrease wing area and structural mass, this effect is offset by reduced aerodynamic performance. The associated increase in fuel mass requires larger inner and transition wing areas, ultimately degrading all key performance metrics. The lateral tank layout is excluded from this analysis, as the corresponding sizing leads to infeasible configurations.

Methodological Assumptions

To evaluate the robustness of the kerosene BWB baseline with respect to key modeling assumptions and methodological uncertainties, a structured sensitivity analysis is conducted. Penalty factors are applied to three principal parameters: passenger density, structural mass, and aircraft drag. These parameters are selected because they represent

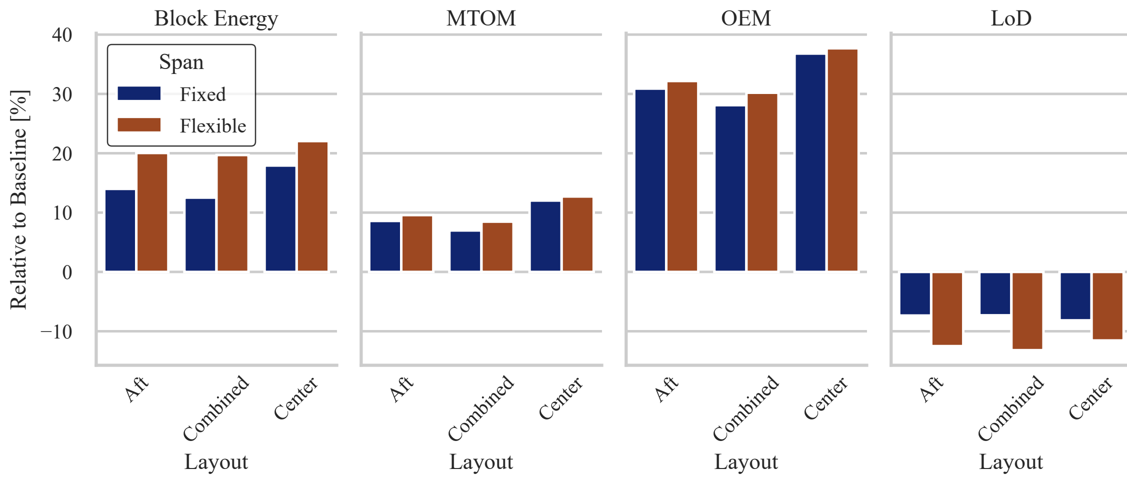

Fig. 19 Sensitivity of LH_2 configurations to fixed wingspan assumption.

major sources of uncertainty at the conceptual design stage and exhibit notable variability across published studies. A structural mass variance of ±1000 kg is applied at the structural mass COG, to reflect differences in structural concepts, or estimation methods. Similarly, aerodynamic performance predictions at the conceptual design level are subject to inherent uncertainty. To assess the sensitivity to aerodynamic discrepancies, a variance of ±5 drag counts (DC) is applied to the zero-lift drag coefficient. For the design of the BWB configurations, a penalty factor of -10 % is applied to the passenger density in order to account for potentially less efficient space utilization inherent to the BWB cabin layout, as well as for geometric idealizations introduced in the modeling of the cabin leading edge. To assess the sensitivity of the results to this assumption, the penalty factor is varied by ±5 %.

Figure 20 illustrates the effects of these changes, showing the relative impact of variations in design parameters on key performance metrics compared to the kerosene BWB baseline. Changes in passenger density, visualized in Fig. 20a, primarily affect the OEM, with minimal impact on aerodynamic performance, resulting in only modest changes in block energy. Increases in passenger density result in a decrease in block energy, while decreases in passenger density result in an increase. A variation of ±5 % in passenger density produces an approximately ±1.5 % change in block energy relative to the kerosene BWB baseline. A similar trend is observed for variations in structural mass, visualized in Fig. 20b. The addition of 1000 kg to the structural mass leads to an increase in block energy of approximately 2 % relative to the kerosene BWB baseline, with the corresponding reduction producing a comparable decrease. The addition of 5 DC to the zero-lift drag results in a significant degradation of aerodynamic efficiency (reduction in the LoD-ratio) and an accompanying increase in block energy of approximately 4 %, visualized in Fig. 20c. Compared to its effect on block energy, the impact of this drag perturbation on OEM and MTOM is minimal.

These sensitivities are, however, of limited importance for the study's conclusions, because the objective is to compare different BWB configurations under the same assumptions and methods. Thus, systematic biases would affect all variants in approximately the same way.

VI. Discussion

For BWB configurations, contextualizing and validating the results against existing literature is particularly important, given the substantial uncertainties inherent in their conceptual design. In the following, the mass breakdown of the selected LH_2 BWB is compared with values reported in the literature. In addition, the corresponding energy consumption results are benchmarked against published data to assess the plausibility and consistency of the present findings.

Comparison of Mass Breakdown to Literature

The mass breakdown of the selected LH_2 BWB is compared with literature values in Table 8. The kerosene configuration by Ahuja et al. [44] is included as a calibration reference, as outlined in Chapter III. To enable comparison across aircraft with differing TLARs, mass fractions relative to MTOM are used. Nevertheless, comparability is limited, since the TLAR summarized at the top of Table 8 differ substantially between the studies.

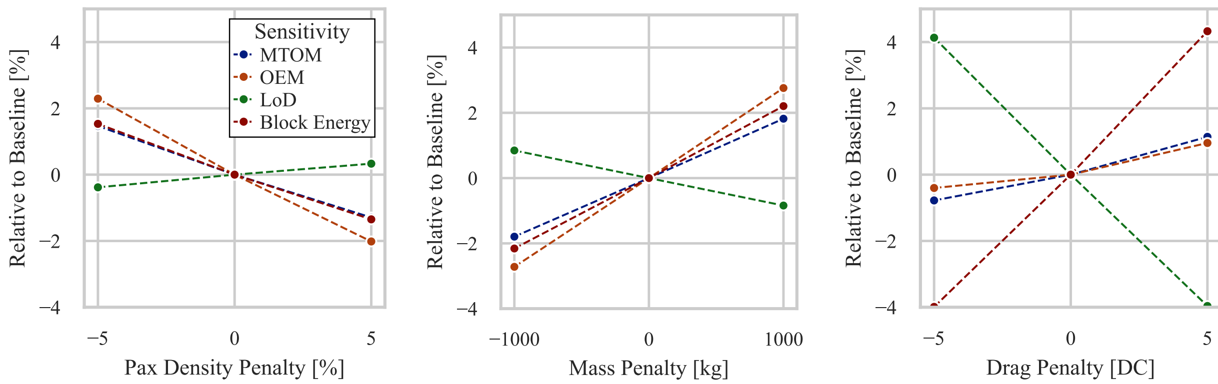

(a) Passenger density. **(b) Mass penalty.** **(c) Drag penalty.**

Fig. 20 Sensitivity of kerosene BWB configuration to methodological assumptions.

Despite these differences, Table 8 reveals notable variations not only between the selected LH_2 BWB and the literature values, but also among the literature sources themselves. Some discrepancies can be attributed to differences in mass bookkeeping conventions. For instance, in the present methodology, unusable fuel is accounted for within operator items, whereas this allocation is not specified consistently in other studies. However, the selected configuration remains within the range reported in the literature, with the exception of a somewhat lower structural mass fraction.

The largest deviation is observed in the cumulative wing mass fraction. This difference is primarily attributable to the application of ambitious technology factors in the present study. The resulting wing mass fraction closely matches that of the calibration aircraft by Ahuja et al. [44]. Similarly, Karpuk et al. [11], who also assume advanced technology factors for the wing structure, report a comparable structural mass fraction. The systems and items mass fraction of the implemented BWB is approximately 0.01–0.02 higher than that of the other LH_2 configurations, with the exception of Di Summa [17], who report a significantly lower value. The OEM fraction lies within the range documented for other LH_2 BWB designs. The fuel mass fraction of the implemented configuration is substantially lower than in most reference cases, except for Patel et al. [15]. This result is consistent with the comparatively shorter design ranges of both Patel's configuration and the present aircraft.

Comparison of Performance to Literature

Figure 21 summarizes the LH_2 integration penalties relative to kerosene baselines reported in previous studies and distinguishes between the underlying tank mass estimation methodologies. In particular, it differentiates between approaches based on physics-based structural models and those relying on prescribed, fixed gravimetric efficiencies. For additional context, corresponding results for TAW configurations are also included. It should be emphasized, however, that the definition and scope of tank gravimetric efficiency are not applied consistently across the literature, which limits the direct comparability of the reported values.

Notably, Adler and Martins [13] and Jagtap et al. [10] assume comparatively high tank gravimetric efficiencies relative to those obtained from physics-based mass estimations. A general trend can be identified: the relative LH_2 integration penalty decreases with increasing mission range. This observation is consistent with the findings of Jagtap et al. [10] and Chan et al. [14], who report lower relative penalties for longer ranges and higher passenger capacities. An exception to this trend is the configuration presented by Karpuk et al. [11], which is broadly comparable to that of Adler and Martins [13] but exhibits a significantly higher integration penalty. Although both studies report similar gravimetric efficiencies for comparable tank layouts, their integration concepts differ substantially. Adler and Martins [13] assume an integral conformal tank integrated within the transition wing, whereas Karpuk et al. [11] model non-integral cylindrical tanks in the same region. This distinction in structural integration likely contributes to the observed differences in integration penalties. Furthermore, the discrepancy between Karpuk et al. [11] and the present study may stem from less efficient volumetric utilization, as Karpuk employs exclusively cylindrical tanks without conical end segments. It is also unclear whether structural and installation clearances were considered, which could otherwise result in optimistic packing assumptions. The results of the present study show good agreement with those of Nguyen Van et al. [12] for a similarly sized LH_2 BWB configuration. Compared with other studies applying physics-based tank mass estimation, the

Table 8 Comparison of LH_2 BWB mass breakdowns as a fraction of MTOM.

Parameter		Implemented BWB	Di Summa [17]	Patel et al. [15]	Karpuk et al. [11]	Adler and Martins [13]	Ahuja et al. [44]
Payload [kg]		25000	35100	11431	70000	52617	25515
Range [nmi]		2500	5400	2200	5720	5500	5000
Inner Wing		0.183	0.281	0.164	0.101	0.185	0.154
Transition Wing		0.029		0.111	0.164	0.175	0.077
Outer Wing		0.038	0.116				
Wing Structure	∑	0.250	0.397	0.276	0.265	0.360	0.231
Landing Gear		0.029	0.041	0.039	0.039	0.054	0.036
Pylons		0.009	-	-	-	-	-
Engines & Nacelles		0.101	0.123	0.172	0.045	0.067	0.086
LH_2 Tanks		0.076	0.071	0.036	0.098	0.069	-
Systems		0.062	0.074	0.087	-	-	0.050
Operator Items		0.089	-	0.036	-	-	0.037
Furnishing		0.042	0.027	0.052	-	-	0.106
Systems & Items	∑	0.193	0.101	0.174	0.172	0.185	0.193
OEM	∑	0.658	0.734	0.696	0.625	0.650	0.510
Payload		0.289	0.135	0.210	0.268	0.247	0.221
Total Fuel		0.054	0.131	0.053	0.107	0.103	0.269
MTOM [kg]	∑	86633	260000	54338	260846	212835	115501

present analysis yields lower gravimetric efficiencies. A contributing factor may be the conservative assumption, in which the tank shell mass is doubled to account for thermal fatigue effects. In addition, the gravimetric efficiency here includes the mass of crash structures, attachment structures, and unusable fuel, leading to a more comprehensive and thus lower efficiency value. As discussed in Chapter V.C, the relative performance of BWB and TAW configurations depends strongly on tank gravimetric efficiency. At lower efficiencies, the BWB demonstrates superior performance, whereas at higher efficiencies the TAW becomes more favorable. This trend is consistent with the findings of Adler and Martins [13], but contrasts with Nguyen Van et al. [12], who report substantially lower LH_2 integration penalties for the BWB than for the TAW across all examined gravimetric efficiencies. Finally, the block energy reduction of approximately 12.5 % observed when transitioning from a kerosene TAW to a kerosene BWB configuration is well aligned with the range reported in the literature for BWB aircraft of comparable size and range [6, 46, 54].

VII. Conclusion

This study assessed the impact of different LH_2 tank layout strategies on the energy performance of a hydrogen-fueled BWB aircraft relative to a kerosene-fueled BWB and a corresponding TAW configuration, all designed under consistent TLAR representative of an Airbus A321neo–class aircraft and assuming a 2050 EIS.

Among the four investigated BWB tank layouts, the combined configuration, with tanks positioned both beside and aft of the passenger cabin, exhibited the lowest hydrogen integration penalty. When geometric effects on tank gravimetric efficiency are consistently accounted for, the LH_2 BWB shows a 12.5 % increase in block energy relative to its kerosene BWB baseline, compared to 10.5 % for the LH_2 TAW. This corresponds to a 2.0 % higher hydrogen integration penalty for the BWB than for the TAW on the design mission. Sensitivity analyses confirm that while absolute values vary with assumptions on tank mass, clearances, and aerodynamic parameters, the relative difference between configurations remains small and robust.

These findings suggest that, the BWB does not provide a clear advantage over the TAW in terms of hydrogen integration. However, the performance gap is modest and likely within the bounds of conceptual-level uncertainty. Moreover, the BWB retains its inherent aerodynamic efficiency advantage over the TAW, achieving a block energy

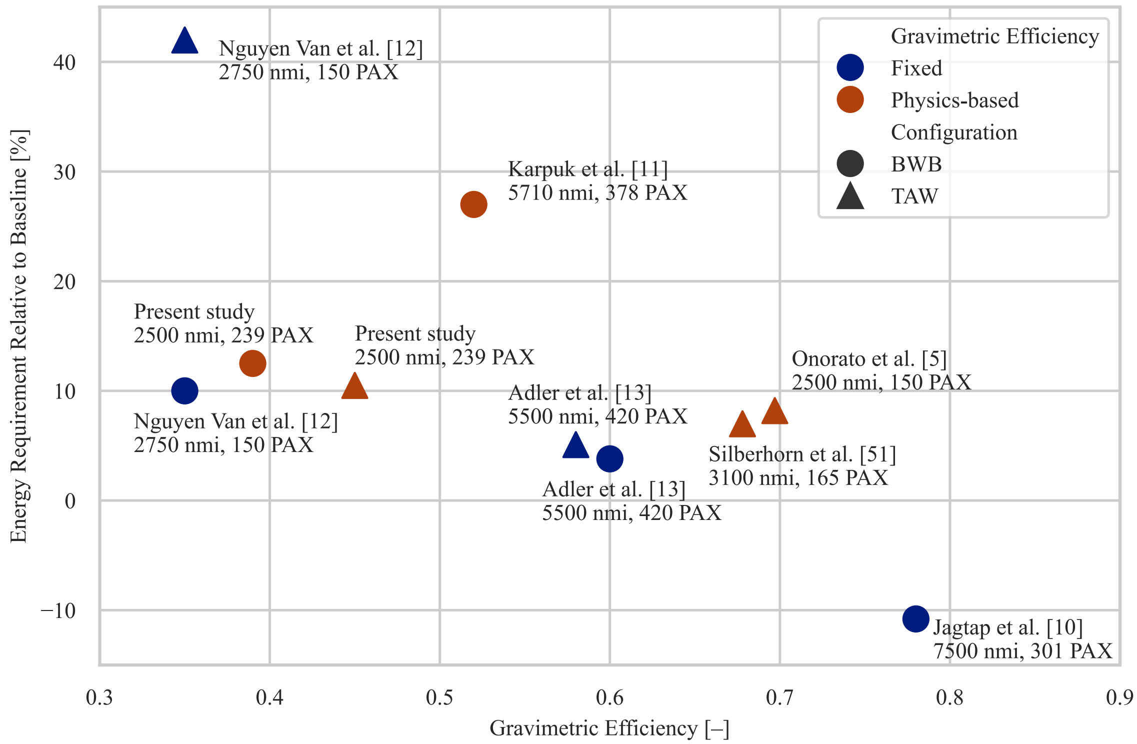

Fig. 21 Comparison of LH_2 integration penalty for the design mission between the selected BWB configuration and results from literature [5, 10–13, 53].

reduction of approximately 12.5 % when comparing kerosene-fueled configurations. Hydrogen integration therefore does not negate the fundamental efficiency potential of the BWB, even if its relative penalty is slightly higher.

The results are specific to the chosen aircraft size and geometric assumptions. For larger BWBs, unused internal volume may accommodate tanks more efficiently, potentially reducing integration penalties. Likewise, alternative design choices, such as increased thickness-to-chord ratios, double-deck cabin arrangements, or more advanced structural concepts, could enable gravimetric efficiencies comparable to those of TAW configurations and shift the balance in favor of the BWB.

Several limitations constrain the present conclusions. The geometric parameterization restricts planform flexibility, particularly in the transition wing region, and may limit optimal tank integration. The use of low-fidelity mass and aerodynamic methods reduces absolute accuracy and design space exploration capability. The automatic tank-fitting algorithm does not consider global optimization of tank size and aircraft scaling. In addition, evacuation constraints are not modeled and may significantly influence feasible tank layouts.

From a design perspective, the combined tank layout emerges as the most promising option within the investigated framework, while lateral and aft layouts remain viable alternatives depending on integration and certification constraints. The center tank layout performs worst in the present assessment, but this result is sensitive to structural modeling assumptions and may improve under alternative structural concepts. Static stability is identified as a key design driver, strongly influenced by outer wing positioning and inner wing sweep, highlighting the tight coupling between aerodynamic layout and hydrogen integration.

Overall, the BWB should not be regarded as an unequivocal solution for hydrogen integration in the SMR segment. Nevertheless, it remains a compelling alternative due to its intrinsic aerodynamic efficiency and its potential for improved tank integration in larger or more geometrically flexible designs. Further investigation using higher-fidelity tools and expanded geometric freedom is required to fully assess its long-term potential.

References

[1] Lee, D. S., Fahey, D. W., Skowron, A., Allen, M. R., Burkhardt, U., Chen, Q., Doherty, S. J., Freeman, S., Forster, P. M., Fuglestvedt, J., Gettelman, A., de León, R. R., Lim, L. L., Lund, M. T., Millar, R. J., Owen, B., Penner, J. E., Pitari, G., Prather,

M. J., Sausen, R., and Wilcox, L. J., "The contribution of global aviation to anthropogenic climate forcing for 2000 to 2018," *Atmospheric Environment*, Vol. 244, 2021, p. 117834. https://doi.org/10.1016/j.atmosenv.2020.117834.

[2] Oesingmann, K., Grimme, W., and Scheelhaase, J., "Hydrogen in aviation: A simulation of demand, price dynamics, and CO2 emission reduction potentials," *International Journal of Hydrogen Energy*, Vol. 64, 2024, pp. 633–642. https://doi.org/10.1016/j.ijhydene.2024.03.241.

[3] Brewer, G. D., *Hydrogen Aircraft Technology*, 1st ed., CRC Press LLC, Boca Raton, Florida, USA, 1991. https://doi.org/10.1201/9780203751480.

[4] Airbus, "Cryoplane: Liquid Hydrogen Fuelled Aircraft - System Analysis," Technical report, Sep. 2003. URL https://web.archive.org/web/20250821084802/https://www.fzt.haw-hamburg.de/pers/Scholz/dglr/hh/text_2004_02_26_Cryoplane.pdf.

[5] Onorato, G., Proesmans, P., and Hoogreef, M. F. M., "Assessment of hydrogen transport aircraft: Effects of fuel tank integration," *CEAS aeronautical journal*, Vol. 13, No. 4, 2022, pp. 813–845. https://doi.org/10.1007/s13272-022-00601-6.

[6] Fröhler, B. M., Iwanizki, M., Woehler, S., and Zill, T., "Increasing Fuel Efficiency for Short to Medium Range Market: A Conceptual Aircraft Design Study on Unconventional Configuration," *AIAA AVIATION FORUM AND ASCEND 2024*, American Institute of Aeronautics and Astronautics, Reston, Virginia, USA, 2024, pp. 1–31. https://doi.org/10.2514/6.2024-4325.

[7] Liebeck, R., Page, M., and Rawdon, B., "Blended-wing-body subsonic commercial transport," *36th AIAA Aerospace Sciences Meeting and Exhibit*, American Institute of Aeronautics and Astronautics, Reston, Virigina, USA, 1998, pp. 1–12. https://doi.org/10.2514/6.1998-438.

[8] Hepperle, M., "The VELA Project," Project summary, DLR, 2005. URL https://web.archive.org/web/20170315224855/http://www.dlr.de/as/Portaldata/5/Resources/dokumente/projekte/vela/The_VELA_Project.pdf.

[9] Winnefeld, C., Kadyk, T., Bensmann, B., Krewer, U., and Hanke-Rauschenbach, R., "Modelling and Designing Cryogenic Hydrogen Tanks for Future Aircraft Applications," *Energies*, Vol. 11, No. 1, 2018, p. 105. https://doi.org/10.3390/en11010105.

[10] Jagtap, S. S., Childs, P. R., and Stettler, M. E., "Conceptual design-optimisation of a subsonic hydrogen-powered long-range blended-wing-body aircraft," *International Journal of Hydrogen Energy*, Vol. 96, 2024, pp. 639–651. https://doi.org/10.1016/j.ijhydene.2024.11.331.

[11] Karpuk, S., Ma, Y., and Elham, A., "Design Investigation of Potential Long-Range Hydrogen Combustion Blended Wing Body Aircraft with Future Technologies," *Aerospace*, Vol. 10, No. 6, 2023, p. 566. https://doi.org/10.3390/aerospace10060566.

[12] Nguyen Van, E., Gauvrit-Ledogar, J., Julien, C., Paluch, B., Ruan, Jiangheng, L, and Moens, F., "Impact of Hydrogen fuel on overall design of transport aircraft," *34th Congress of the International Council of the Aeronautical Sciences*, International Council of the Aeronautical Sciences, Florence, Italy, 2024, pp. 1–13. URL https://www.icas.org/icas_archive/icas2024/data/papers/icas2024_0826_paper.pdf.

[13] Adler, E. J., and Martins, J. R. R. A., "Blended Wing Body Configuration for Hydrogen-Powered Aviation," *Journal of Aircraft*, Vol. 61, No. 3, 2024, pp. 887–901. https://doi.org/10.2514/1.C037582.

[14] Chan, J. L., Sun, Y., and Smith, H., "Conceptual Designs of Blended Wing Body Aircraft for the Application of Alternative Fuels," *AIAA AVIATION FORUM AND ASCEND 2024*, American Institute of Aeronautics and Astronautics, Reston, Virginia, USA, 2024, p. 0. https://doi.org/10.2514/6.2024-3989.

[15] Patel, S., Ragauss, E., Ahuja, J., Gladin, J. C., and Mavris, D. N., "Development of a Regional Blended Wing Body Aircraft with Distributed Hybrid Hydrogen-Electric Propulsion," *AIAA SCITECH 2024 Forum*, American Institute of Aeronautics and Astronautics, Reston, Virginia, USA, 2024, p. 0. https://doi.org/10.2514/6.2024-0282.

[16] Wilod Versprille, V., "Aerodynamic Shape Optimization of a Liquid-Hydrogen-Powered Blended-Wing-Body," M.sc. thesis, Delft University of Technology, Delft, The Netherlands, 2022. URL https://resolver.tudelft.nl/uuid:08fbb7f6-64c0-4262-a67a-df20d0a52cde.

[17] Di Summa, G., "The Effect of the Internal Layout of Hydrogen Combustion Blended Wing Body Concepts on Performance," M.sc. thesis, Delft University of Technology, Delft, The Netherlands, 2025. URL https://resolver.tudelft.nl/uuid:21494bbc-7149-45bb-bad3-7d6a62408231.

[18] Warwick, G., Norris, G., and Dubois, T., "Airbus ZEROe Plan Postponement Cools Prospects For Hydrogen Propulsion," *Aviation Week Network*, Feb. 2025. URL https://web.archive.org/web/20250821124732/https://aviationweek.com/aerospace/emerging-technologies/airbus-zeroe-plan-postponement-cools-prospects-hydrogen-propulsion.

[19] Airbus, "Airbus reveals new zero-emission concept aircraft," Press release, Oct. 2021. URL https://web.archive.org/web/20250820142753/https://www.airbus.com/en/newsroom/press-releases/2020-09-airbus-reveals-new-zero-emission-concept-aircraft.

[20] Sampson, B., "JetZero selects flight control suppliers for its blended wing aircraft," *Aerospace Testing International*, Nov. 2024. URL https://web.archive.org/web/20250821092136/https://www.aerospacetestinginternational.com/news/jetzero-selects-flight-control-suppliers-for-its-blended-wing-aircraft.html.

[21] Adler, E. J., and Martins, J. R., "Hydrogen-powered aircraft: Fundamental concepts, key technologies, and environmental impacts," *Progress in Aerospace Sciences*, Vol. 141, 2023, p. 100922. https://doi.org/10.1016/j.paerosci.2023.100922.

[22] Boden, B., Flink, J., Först, N., Mischke, R., Schaffert, K., Weinert, A., Wohlan, A., and Schreiber, A., "RCE: An Integration Environment for Engineering and Science," *SoftwareX*, Vol. 15, 2021, p. 100759. https://doi.org/10.1016/j.softx.2021.100759.

[23] Alder, M., Moerland, E., Jepsen, J., and Nagel, B., "Recent Advances in Establishing a Common Language for Aircraft Design with CPACS," *Aerospace Europe Conference*, Council of European Aerospace Societies, Bordeaux, France, 2020, pp. 1–14. URL https://elib.dlr.de/134341/.

[24] Wöhler, S., Atanasov, G., Silberhorn, D., Fröhler, B., and Zill, T., "Preliminary Aircraft Design within a Multidisciplinary and Multifidelity Design Environment," *Aerospace Europe Conference*, Council of European Aerospace Societies, Bordeaux, France, 2020, pp. 1–12. URL https://elib.dlr.de/185515/.

[25] Raymer, D. P., *Aircraft design: A conceptual approach*, AIAA education series, American Institute of Aeronautics and Astronautics Inc, Reston, Virginia, USA, 2018. https://doi.org/10.2514/4.104909.

[26] Torenbeek, E., *Synthesis of Subsonic Airplane Design*, Delft University Press, Kluwer Academic Publishers, Delft, The Netherlands, 1982. https://doi.org/10.1007/978-94-017-3202-4.

[27] Roskam, J., *Airplane Design Part I-VII*, DARcorporation, Lawrence, Kansas, USA, 2008.

[28] IABG mbH, *Luftfahrttechnisches Handbuch*, LTH-Koordinierungsstelle, 2018. URL https://www.lth-online.de/.

[29] Balack, P., Hecken, T., Petsch, M., Atanasov, G., and Silberhorn, D., "Semi-Physical Method for the Mass Estimation of Fuselages Carrying Liquid Hydrogen Fuel Tanks in Conceptual Aircraft Design," *Deutscher Luft- und Raumfahrtkongress 2022*, Deutsche Gesellschaft für Luft- und Raumfahrt - Lilienthal-Oberth e.V, Dresden, Germany, 2022, pp. 1–6. https://doi.org/10.25967/570315.

[30] Torenbeek, E., *Advanced Aircraft Design - Conceptual Design, Analysis and Optimization of Subsonic Civil Airplanes*, Wiley, Chichester, United Kingdom, 2013. https://doi.org/10.1002/9781118568101.

[31] Bradley, K. R., and Kimmel, W. M., "A Sizing Methodology for the Conceptual Design of Blended-Wing-Body Transports," Contractor report, NASA, Sep. 2004. URL https://ntrs.nasa.gov/citations/20040110949.

[32] Howe, D., "Blended wing body airframe mass prediction," *Proceedings of the Institution of Mechanical Engineers, Part G: Journal of Aerospace Engineering*, Vol. 215, No. 6, 2001, pp. 319–331. https://doi.org/10.1243/0954410011533329.

[33] Howe, D., "The Prediction of Aircraft Wing Mass," *Proceedings of the Institution of Mechanical Engineers, Part G: Journal of Aerospace Engineering*, Vol. 210, No. 2, 1996, pp. 135–145. https://doi.org/10.1243/PIME_PROC_1996_210_355_02.

[34] de Castro, H. V., "The longitudinal static stability of tailless aircraft," Cranfield University, Report, 2001. URL http://hdl.handle.net/1826/228.

[35] Burschyk, T., Fröhler, B., Alder, M., and Zill, T., "Global Sensitivity Analysis of Liquid Hydrogen Storage Design Parameters for Overall Aircraft Design," *34th Congress of the International Council of the Aeronautical Sciences*, International Council of the Aeronautical Sciences, Florence, Italy, 2024, pp. 1–21. URL https://www.icas.org/icas_archive/icas2024/data/papers/icas2024_0092_paper.pdf.

[36] Freund, S., Burschyk, T., Jacobsen, L., and Franzoni, F., "Automated Structural Design Optimization of Double Walled Liquid Hydrogen Tanks and Subsequent Comparison of CFRP with Aluminium on Aircraft Level," *Deutscher Luft- und Raumfahrtkongress 2025*, Deutsche Gesellschaft für Luft- und Raumfahrt - Lilienthal-Oberth e.V, Augsburg, Germany, 2025, pp. 1–4. URL https://elib.dlr.de/219055/.

[37] Freund, S., Lueders, C., Jacobsen, L., and Franzoni, F., "tankoh2," Software, German Aerospace Center, 2025. URL https://gitlab.com/DLR-SY/tank/tankoh2.

[38] Sielemann, M., Renuke, A., O'Donovan, K., Andersson, D., and Nguyen, A., "On Tank and Dormancy Design Spaces for Hydrogen Powered Aircraft," *AIAA SCITECH 2025 Forum*, American Institute of Aeronautics and Astronautics, Reston, Virginia, USA, 2025, p. 0. https://doi.org/10.2514/6.2025-0504.

[39] Airbus S.A.S, "A321: Aircraft Characteristics Airport and Maintenance Planning," Manual, Dec. 2023. URL https://web.archive.org/web/20250720152032/https://aircraft.airbus.com/sites/g/files/jlcbta126/files/2023-12/ac_a321_1223.pdf.

[40] Wöhler, S., Häßy, J., and Kriewall, V., "Establishing the DLR-F25 as a Research Baseline Aircraft For the Short-Medium Range Market in 2035," *34th Congress of the International Council of the Aeronautical Sciences*, International Council of the Aeronautical Sciences, Florence, Italy, 2024, pp. 1–28. URL https://www.icas.org/icas_archive/icas2024/data/papers/icas2024_0398_paper.pdf.

[41] Fröhler, B. M., Alder, M., Woehler, S., and Zill, T., "Assessing Uncertainties of an Evolutionary Baseline as Benchmark of Future Aircraft Designs," *AIAA SCITECH 2024 Forum*, American Institute of Aeronautics and Astronautics, Orlando, Florida, USA, 2024, pp. 1–23. https://doi.org/10.2514/6.2024-2813.

[42] Weber, L., Szöke-Erös, H., Ratei, P., and Shiva Prakasha, P., "A Technlogy Scouting and Roadmapping Approach of Future Commercial Passenger Aircraft," *Deutscher Luft- und Raumfahrtkongress 2024*, Deutsche Gesellschaft für Luft- und Raumfahrt - Lilienthal-Oberth e.V, Hamburg, Germany, 2024, pp. 1–11. https://doi.org/10.25967/630333.

[43] Kuntzagk, S., "Aeroshark – Drag Reduction Using Riblet Film on Commercial Aircraft," Presentation, Lufthansa Technik, 2024. https://doi.org/10.5281/ZENODO.11214243.

[44] Ahuja, J., Perron, C., Bermudez Rivera, R. D., Tai, J. C., and Mavris, D. N., "Comparison of blended wing body and tube-and-wing performance characteristics," *The Aeronautical Journal*, 2025, pp. 1–27. https://doi.org/10.1017/aer.2025.8.

[45] Kawai, R. T., "Acoustic Prediction Methodology and Test Validation for an Efficient Low-Noise Hybrid Wing Body Subsonic Transport," Report, NASA Langley Research Center, The Boeing Company Boeing Research and Technology, Feb. 2011. URL https://ntrs.nasa.gov/citations/20130014003.

[46] Brown, M., and Vos, R., "Conceptual design and evaluation of blended-wing-body aircraft," *AIAA Aerospace Sciences Meeting*, American Institute of Aeronautics and Astronautics, Reston, Virginia, USA, 2018, pp. 1–22. https://doi.org/10.2514/6.2018-0522.

[47] Velicki, A., Thrash, P., and Jegley, D., "Airframe Development for the Hybrid Wing Body Aircraft," *47th AIAA Aerospace Sciences Meeting including The New Horizons Forum and Aerospace Exposition*, American Institute of Aeronautics and Astronautics, Reston, Virigina, USA, 2009, p. 0. https://doi.org/10.2514/6.2009-932.

[48] Burschyk, T., Silberhorn, D., Wehrspohn, J., Kühlen, M., and Zill, T., "Scenario-based implications of liquid hydrogen storage tank insulation quality for a short-range aircraft concept," *AIAA AVIATION 2023 Forum*, American Institute of Aeronautics and Astronautics, Reston, Virginia, USA, 2023, pp. 1–21. https://doi.org/10.2514/6.2023-3522.

[49] Sutton, G. P., and Biblarz, O., *Rocket propulsion elements*, ninth edition ed., John Wiley & Sons Inc, Hoboken, New Jersey, 2017.

[50] Kotzem, M., Wöhler, S., Burschyk, T., Hesse, C., Hellbrück, S., and Zill, T., "Conceptual Aircraft Design of a Research Baseline with Direct Liquid Hydrogen Combustion," *34th Congress of the International Council of the Aeronautical Sciences*, International Council of the Aeronautical Sciences, Florence, Italy, 2024, pp. 1–21. URL https://www.icas.org/icas_archive/icas2024/data/papers/icas2024_0503_paper.pdf.

[51] Görtz, A., and Schneider, B., "Step-by-Step Evaluation of the Fuel Switch From Kerosene to Hydrogen on the Thermodynamic Cycle in Gas Turbine Engines," *Journal of Engineering for Gas Turbines and Power*, Vol. 146, No. 11, 2024. https://doi.org/10.1115/1.4065926.

[52] European Commission, "SMR aircraft architecture and technology integration project: Grant agreement ID: 101101955," , April 2026. https://doi.org/10.3030/101101955, URL https://cordis.europa.eu/project/id/101101955.

[53] Silberhorn, D., Atanasov, G., Walther, J.-N., and Zill, T., "Assessment of Hydrogen Fuel Tank Integration at Aircraft Level," *Deutscher Luft- und Raumfahrtkongress 2019*, Darmstadt, Deutschland, 2019, p. 0. URL https://elib.dlr.de/129643/.

[54] Dorsey, A., and Uranga, A., "Design Space Exploration of Blended Wing Bodies," *AIAA AVIATION 2021 FORUM*, American Institute of Aeronautics and Astronautics, Reston, Virginia, USA, 2021, pp. 1–20. https://doi.org/10.2514/6.2021-2422.